Chemical Engineering Science 128 (2015) 130–146

Contents lists available at ScienceDirect

Chemical Engineering Science

journal homepage: www.elsevier.com/locate/ces

Analysis of the cyanobacterial hydrogen photoproduction process via model identification and process simulation

Dongda Zhang [a], Pongsathorn Dechatiwongse [b], Ehecatl Antonio Del-Rio-Chanona [a], Klaus Hellgardt [b], Geoffrey C. Maitland [b], Vassilios S. Vassiliadis [a,*]

[a] Department of Chemical Engineering and Biotechnology, University of Cambridge, Pembroke Street, Cambridge CB2 3RA, UK
[b] Department of Chemical Engineering, Imperial College London, South Kensington Campus, London SW7 2AZ, UK

HIGHLIGHTS

- Dynamic simulation models for cyanobacterial hydrogen production process.
- Parameter estimation via dynamic optimisation.
- Proposed modified models exhibit higher accuracy for real process simulation.
- Interpretation of higher performance of CSTR over PFR for this process.
- Fed-batch processes are proposed as the optimal reactor operation.

ARTICLE INFO

Article history:
Received 1 October 2014
Received in revised form
9 January 2015
Accepted 24 January 2015
Available online 2 February 2015

Keywords:
Biohydrogen
Cyanobacteria
Photoproduction
Kinetic models
Process simulation
Bioreactor design

ABSTRACT

Cyanothece sp. ATCC 51142 is considered a microorganism with the potential to generate sustainable hydrogen in the future. However, few kinetic models are capable of simulating different phases of *Cyanothece* sp. ATCC 51142 from growth to hydrogen production. In the present study four models are constructed to simulate *Cyanothece* sp. batch photoproduction process. A dynamic optimisation method is used to determine parameters in the models. It is found that although the piecewise models fit experimental data better, large deviation can be induced when they are used to simulate a process whose operating conditions are different from the current experiments. The modified models are eventually selected in the present study to simulate a two-stage continuous photoproduction process. The current simulation results show that a plug flow reactor (PFR) shows worse performance compared to a continuous stirred-tank reactor (CSTR) in the current operating conditions since it lowers the total hydrogen production. The finding is that nitrate and oxygen concentration change along the direction of culture movement in PFR, and hydrogen is only generated in the zone where both of them are low. The reactor area thereby is not well utilised. Additionally, as hydrogen production rate is primarily influenced by biomass concentration, which increases initially and decreases eventually along the direction of culture movement, the overall hydrogen production rate in a PFR may be lower than that in a CSTR. Finally, in this study fed-batch photoproduction processes are proposed containing only one photo-bioreactor based on the current simulation.

1. Introduction

1.1. Introduction of biohydrogen production from different microorganisms

Molecular hydrogen (H_2) is considered as one of the fuels of the future with greatest potential and environmental friendliness. At present, the conventional industrial hydrogen production process almost totally relies upon the utilisation of carbon-based resources which are limited and not renewable (Cooke et al., 2011). In order to fulfill the world's long-term energy needs, it is essential to find low cost, sustainable and environmentally friendly resources for future hydrogen production. Recently biohydrogen, the hydrogen produced by microorganism biosynthesis, has been extensively investigated due to its outstanding advantages. For example, the energy source of biohydrogen is solar energy, which is always plentiful and has a low investment cost (Catalanotti et al., 2013). Although biohydrogen can be generated by different microorganisms, two groups, photosynthetic green algae and nitrogen-fixing cyanobacteria, are particularly of interest, since they can photosynthetically

* Corresponding author. Tel.: +44 1223 330142.
E-mail address: vsv20@cam.ac.uk (V.S. Vassiliadis).

http://dx.doi.org/10.1016/j.ces.2015.01.059

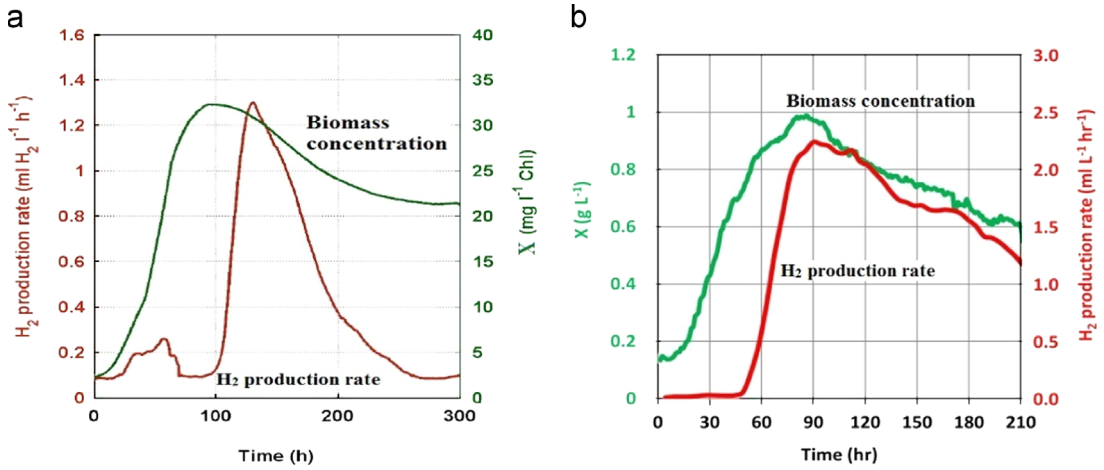

Fig. 1. Comparison of green algal and cyanobacteria hydrogen production rate. (a) Hydrogen production rate and biomass concentration during the time course of photoproduction reported by Tamburic et al. (2012) in green algae. (b) Hydrogen production rate and biomass concentration during the time course of photoproduction reported by Dechatiwongse et al. (2015) in cyanobacteria.

derive H_2 from sunlight (Catalanotti et al., 2013; Min and Sherman, 2010).

Chlamydomonas reinhardtii, an outstanding representative of green algae, has been extensively explored. Previous research demonstrated that in *C. reinhardtii* hydrogen is generated by hydrogenase (Melis et al., 2000). Electrons for hydrogen reduction are originally provided by water through photosynthesis with the generation of oxygen. As the activity of hydrogenase is completely inhibited by oxygen, *C. reinhardtii* can only produce hydrogen in anaerobic conditions (Antal et al., 2011). Different methods have been used to remove oxygen in algal culture, while the generally accepted method in recent research is to cultivate *C. reinhardtii* in a sulphur-free culture (Melis et al., 2000). As algal photosynthetic activity is significantly inhibited without the replenishment of sulphur, oxygen production rate is significantly reduced and even drops lower than algal respiration rate. Hence, oxygen produced by oxygenic photosynthesis is totally consumed by algae respiration and anaerobic conditions are achieved.

In addition to hydrogenase, Bandyopadhyay et al. (2010) finds that cyanobacteria also process nitrogenase for hydrogen production. *Cyanothece* sp. ATCC 51142 is mainly selected as the typical cyanobacteria in the current research because its remarkably high rate of H_2 production has never been observed before in any other hydrogen-producing strains. In spite of having two distinct biological enzymes, previous research has demonstrated that the hydrogen generation rate catalysed by nitrogenase is much higher (Min and Sherman, 2010). In cyanobacteria, hydrogen reduction by nitrogenase is directed by the nitrogen-fixing metabolic pathway instead of photosynthesis, and electrons for hydrogen production are usually provided by the carbohydrate reserved during photosynthesis, or by an additional carbon source such as glycerol (Tripp et al., 2010; Bandyopadhyay et al., 2010). As cyanobacterial nitrogenase activity is inhibited by oxygen and nitrogen source such as nitrate, hydrogen is usually generated in oxygen and nitrogen deprived cultures. Once the activity of nitrogenase is stimulated, hydrogen reduction by nitrogenase can last for a long period even in the absence of nitrogen gas (Kufryk, 2013; Min and Sherman, 2010).

Compared to green algae, cyanobacteria are given more attention in current research because of their distinctive advantages. For example, the profile of cells growth and hydrogen production of both green algae and cyanobacteria are presented in Fig. 1. It is found that because of the dramatic damage of photosynthesis activity in green algae, the decreasing tendency of hydrogen production and cell growth rates in *C. reinhardtii* is much sharper than that in *Cyanothece* sp. ATCC 51142 (Dechatiwongse et al., 2015; Tamburic et al., 2012, 2013). Furthermore, hydrogen production in cyanobacteria is much higher than that in green algae. For example Dechatiwongse et al. (2015) compared the capacity of different microorganisms on hydrogen production, and it is found that the maximum hydrogen productivity of *C. reinhardtii* is only 6.4 μmol mg Chl^{-1} h^{-1}, which is much less than 225 μmol mg Chl^{-1} h^{-1} of *Cyanothece* sp. ATCC 51142. Apart from the higher H_2 production rate cyanobacteria can also utilise nitrogen gas as the nitrogen source, which offers the benefit in terms of significant reduction in nutrient cost. As a result, cyanobacteria are more suitable for industrial biohydrogen production processes.

Extensive research has been conducted to improve the performance of cyanobacteria hydrogen production. For instance, effects of different nutrients and illumination duration on cyanobacterial growth rate and hydrogen productivity have been widely explored (Min and Sherman, 2010; Bandyopadhyay et al., 2010). However, problems such as the influence of light intensity and light wavelength, optimal ratio of nitrogen source to biomass concentration and photobioreactor configuration are still unsolved and restrict the application of hydrogen production by cyanobacteria.

One way to understand the source of these problems is to construct an accurate kinetic model for cyanobacteria photoproduction process simulation and optimisation. Although various kinetic models have been developed such as the Monod model and the logistic model (Xie et al., 2012; Bezerra et al., 2008; Dechatiwongse et al., 2014), most of them are unable to simulate the entire growth phase of cyanobacteria. For example, the Monod model cannot be used to simulate the decay phase of green algae and cyanobacteria where hydrogen is mainly generated (Antal et al., 2011; Melis et al., 2000). The logistic model assumes that bacterial growth is only a function of bacterial biomass concentration, which makes it impossible to explore the influence of limiting nutrients on bacterial growth (Bezerra et al., 2008).

This study aims to construct an accurate kinetic model capable of simulating different cyanobacterial growth phases for hydrogen production. Based on the kinetic model the current research studies the capacity of different cyanobacterial photoproduction processes, including batch operation, fed-batch operation and continuous operation. In order to maximise hydrogen production in different modes of photobioreactor operation, future work will also optimise the operating conditions of each photoproduction process and the configuration of the photobioreactor.

1.2. Growth phases of cyanobacteria

As green algae and cyanobacteria can only generate a significant amount of hydrogen in sulphur or nitrogen deprived cultures,

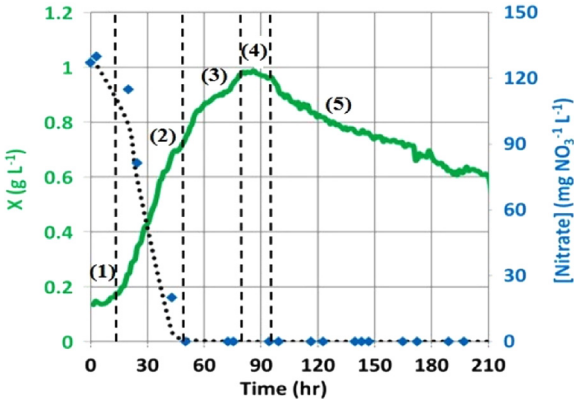

Fig. 2. Growth phases of cyanobacteria. (1) Lag phase; (2) first growth phase where nutrients are presented; (3) second growth phase after nitrate runs out; (4) stationary phase; and (5) decay phase. This experimental research was reported by Dechatiwongse et al. (2015). The solid line represents biomass concentration and the dashed line represents nitrate concentration.

the growth phases of both cyanobacteria and green algae in nutrient limiting cultures are very complicated. Earlier published research found that the growth tendency of green algae and cyanobacteria in terms of time are very similar (Tamburic et al., 2012; Melis et al., 2000; Dechatiwongse et al., 2015). In the current research the growth profile is divided into five growth phases regulated by different metabolic mechanisms and shown in Fig. 2.

When cells are initially incubated in the fresh medium where both nitrate (nitrogen source) and carbon source (glycerol) are present, there is no significant increase of biomass concentration because cells have to adapt themselves to the new growth environment. This brief period is known as “lag phase”. After the adaption period, cells start to grow and biomass concentration increases simultaneously with the decline of both nitrogen source and carbon source. This period is usually termed as “exponential growth phase” (first growth phase) and lasts until the depletion of nitrate.

After nitrate is completely consumed, cyanobacteria continue growing for a period because the nitrogen source has been reserved in cells during the first growth phase. This period is named as the “ second growth phase”, which is much shorter than the first growth phase. During the second growth phase, cell growth rate is decreasing due to the continuous consumption of intracellular nutrients, and this phase finishes when the bacterial growth rate has decreased to a point at which it intercepts the decay rate. A short stationary phase then follows, caused by the similarity in the rate of cell growth and cell decay. After the concentration of intracellular nitrogen source drops to its minimum threshold, cells stop growing and the bacterial decay phase is observed.

Among these five growth phases, hydrogen is only produced from the second growth phase to the decay phase, because the activity of nitrogenase is inhibited in the first growth phase. Its activity is not able to recover until oxygen is exhausted and nitrate concentration is lower than a specific threshold (100 mg L^{-1} observed in the current experimental research) in the culture. However, the first growth phase is also important for cyanobacterial biohydrogen photoproduction as cyanobacteria mainly grow in this phase, and a high biomass concentration is vital for obtaining high hydrogen production. Therefore, all of the four phases should be included in the current simulation research. The current research aims to construct dynamic models for the simulation of cyanobacterial hydrogen production process. Specifically, the cultivation condition is chosen as the photo-heterotrophic growth condition, as glycerol is supplied to suppress photosynthetic activity and enhance hydrogen production rate (Tripp et al., 2010; Bandyopadhyay et al., 2010).

2. Material and methods

2.1. Experimental setup

The culture of *Cyanothece* 51142, purchased from the American Type Culture Collection (ATCC), was grown in an artificial seawater medium–ASP2 (Provasoli et al., 1957) with the addition of 1.5 g L^{-1} $NaNO_3$ and 10 mM of glycerol (99% purity) from Sigma–Aldrich in 250 ml sterile Corning flasks at 30°C, pH of 7.4, under continuous cool-white fluorescent illumination of 10 Wm^{-2} (46 μ E m^{-2} s^{-1}). With 5 days of cultivation, cells achieved their maximum concentration and were then used for inoculation in either batch or chemostat experimental processes. Detailed illustration of the current experimental work can be found in Dechatiwongse et al. (2015).

2.2. Data selection

Two sets of experiments were conducted in a flat plate photobioreactor (PBR). The first set was conducted as a short term batch photoproduction process lasting for 210 h for cyanobacteria hydrogen production. All the cyanobacterial growth phases including lag phase, exponential phase, stationary phase (short) and decay phase were observed in the experiment (Fig. 2).

The second set of experiments executed a continuous process which was switched at the 75th hour from batch mode to continuous production mode. During the first 75 hours of batch mode operation, cyanobacterial growth phases including the lag phase and the growth phases were observed. As the first set of experiments includes the whole growth cycle, experimental data in this set are chosen to estimate parameters in each model. Data in the second set of experiments are then used to verify the accuracy of different models.

2.3. Challenges of model design

Various kinetic models have been constructed to simulate microorganism fermentation processes (Xie et al., 2012; Fouchard et al., 2009; Obeid et al., 2009). Among them the Monod model and the Droop model are widely employed (Vatcheva et al., 2006). Other models which are modified from the Monod model and the Droop model such as the Contois model and the Luedeking–Piret models are designed to improve the accuracy of simulation results (Vatcheva et al., 2006; Obeid et al., 2009). However the challenges in the current research require modifications and even novel methods to be applied on these models for cyanobacteria photoproduction simulation.

Due to the distinctive characters of different cyanobacterial growth phases, it is difficult to design a kinetic model capable of simulating all of them. Particularly in the present study the second growth phase, the stationary phase and the decay phase have to be included as hydrogen is produced in these phases. Meanwhile, the cyanobacterial first growth phase is also of high importance because both oxygen and nitrate are consumed in this phase, and biomass concentration which mainly increases in this phase predominantly determines cyanobacteria hydrogen production rate. Hence all of the growth phases except the lag phase have to be included in the current research, which makes the design of kinetic models much more complicated.

Another challenge is that simpler strategies to discretise differential equations (i.e. Implicit Euler) are inadequate for the high nonlinearity of the proposed models in this work. To ensure the accuracy of the current models, a high order implicit discretisation strategy (equivalent to fourth order implicit Runge–Kutta method)

has been utilised in its place. To simplify the model, recent research (Zhang et al., under review) proposed a piecewise model which decomposes kinetic models into different sub-models corresponding to each growth phase. Parameters in each sub-model therefore can be accurately calculated from experimental data. Eventually different sub-models can be combined by switch functions which are similar to the Heaviside step function, but are differentiable. Even in this case, attention has to be paid on a widely accepted fact that large deviations may be induced when a model is used to simulate a process whose operating conditions are quite different to those of the experiments.

In order to simulate most of the cyanobacterial growth phases and accurately predict the performance of unknown photoproduction processes, in this study two modified models and two piecewise models are constructed and analysed.

2.4. Construction of modified models

Two models modified from the Droop model and the Contois model are constructed in the present study. Details of the methodology employed are presented in the following subsections.

2.4.1. The modified Droop model

The Droop model is a classical model used for fermentation process simulation (Vatcheva et al., 2006). Compared to other kinetic models the Droop model assumes that microorganism growth rate is affected by limiting nutrients in both liquid culture and inside cells, hence it is able to simulate the second growth phase where bacteria keep growing by consuming the intracellular nitrogen source. The intracellular nutrient concentration in the Droop model is always represented as nutrient quota, Q (mg nutrient/g biomass), which is defined as the mass ratio of intracellular nutrient to biomass (Vatcheva et al., 2006). Eq. (1a) is used to calculate microorganism growth rate in the original Droop model where X denotes biomass concentration, and $f(Q)$, calculated by Eq. (1b), denotes the influence of nutrient quota on the growth rate:

$$\frac{dX}{dt} = \mu_{max} \cdot f(Q) \cdot X \tag{1a}$$

$$f(Q) = 1 - \frac{k_Q}{Q} \tag{1b}$$

Three modifications are made here to the Droop model. First of all, a normalised nitrogen quota defined in Eq. (2) is used to replace the unmeasured absolute nitrogen quota. Similarly, to align to the experimental results, the unit of oxygen concentration is set as % saturation O_2.

$$q = \frac{Q}{Q_0} \tag{2}$$

where Q_0 represents the absolute nitrogen quota of *Cyanothece* sp. ATCC 51142 when there is sufficient nitrate and glycerol in the culture.

Secondly, the production rate of fermentation product in the original Droop model is calculated by Eq. (3), which is assumed to be proportional to microorganism growth rate. Because in the current case cyanobacteria can continuously generate hydrogen from the second growth phase to the decay phase, the original Droop model has to be modified. As a result, Eq. (3) is modified to Eq. (4f) which originates from the Luedeking–Piret model (Obeid et al., 2009):

$$\frac{dP}{dt} = Y_{P/X} \cdot \frac{S}{S+K_S} \cdot X \tag{3}$$

Eqs. 4 (a–f) show the details of the Droop model.

Finally, a new term to account for biomass decay is added to the original Droop model. In Eq. (4a) the first term on the right represents the growth rate, and the second term represents the respiration rate. This modification originates from the Logistic model which proposes a respiration rate of second order to biomass concentration for cyanobacteria (Dechatiwongse et al., 2014). Thus the Droop model is able to simulate a photoproduction process from the first growth phase to the decay phase:

$$\frac{dX}{dt} = \mu_{max} \cdot \left(1 - \frac{k_q}{q}\right) \cdot \frac{C}{C+K_C} \cdot X - \mu_d \cdot X^2 \tag{4a}$$

$$\frac{dN}{dt} = -Y_{N/X} \cdot \mu_{max} \cdot \frac{N}{N+K_N} \cdot \frac{C}{C+K_C} \cdot X \tag{4b}$$

$$\frac{dq}{dt} = \mu_{max} \cdot \frac{C}{C+K_C} \cdot \left(Y_{q/X} \cdot \frac{N}{N+K_N} - \left(1 - \frac{k_q}{q}\right) \cdot q\right) \tag{4c}$$

$$\frac{dC}{dt} = -Y_{C/X} \cdot \mu_{max} \cdot \left(1 - \frac{k_q}{q}\right) \cdot \frac{C}{C+K_C} \cdot X \tag{4d}$$

$$\frac{dO}{dt} = Y_{O/X} \cdot \mu_{max} \cdot \frac{N}{N+K_N} \cdot \frac{C}{C+K_C} \cdot X - Y_d \cdot \mu_d \cdot X^2 \cdot f(O) \tag{4e}$$

$$\frac{dH}{dt} = \left(K_{H_2,1} \cdot \frac{dX}{dt} + K_{H_2,2} \cdot X\right) \cdot f(N) \cdot (1 - f(O)) \tag{4f}$$

where N represents the nitrate concentration in the culture, q represents the intracellular nitrogen quota, C represents the glycerol concentration, O represents the oxygen concentration, and H represents the hydrogen production.

The current experimental work leads to the observation that the activity of nitrogenase is only recovered when the culture is anaerobic and nitrate concentration is lower than 100 mg L^{-1}. The switch functions in Eqs. (5) and (6) are used to regulate the start and termination of hydrogen production. Similarly because the consumption of oxygen by cyanobacterial respiration is a complex process, Eq. (6) has to be applied to prevent the simulated oxygen concentration from becoming negative.

$$f(N) = 0.5 \cdot \frac{\left((N-100)^2\right)^{0.5} - (N-100)}{\left[(N-100)^2 + 0.1\right]^{0.5}} \tag{5}$$

$$f(O) = \frac{O}{\left(O^2 + 0.1\right)^{0.5}} \tag{6}$$

When the culture is anaerobic ($O = 0$) and nitrate concentration is lower than its threshold ($N < 100$ mg L^{-1}) hydrogen is generated ($f(N) = 1$ and $f(O) = 0$); otherwise hydrogen production is inhibited ($f(N) = 0$ or $f(O) = 1$).

2.4.2. The modified Contois model

The Contois model can be considered as an improvement of the Droop model Vatcheva et al. (2006). Based on the Droop model, microorganisms will continue growing as long as nutrients are sufficient. However, in reality microorganisms can never grow permanently in a culture even if nutrients are always in excess. The reason why cells stop growing varies among species, and in general biomass growth rate decreases with the increasing biomass concentration. To take this factor into account, in the Contois model the half-velocity constant is replaced by $K_S \cdot X$, shown in Eq. (7), which increases with increasing biomass concentration. As a result, microorganism growth rate decreases with increasing biomass concentration since the term $S/(S+K_S \cdot X)$ decreases with increasing biomass concentration. Therefore the Contois model has a higher accuracy when biomass concentration is high.

Eqs. 8(a–f) show the details of the Contois model. Parameters in the Contois model have the same meaning as those in the Droop

model in Section 2.4.1:

$$\frac{dS}{dt} = -Y_S \cdot \frac{S}{S+K_S \cdot X} \cdot X \tag{7}$$

where S represents the substrate concentration:

$$\frac{dX}{dt} = \mu_{max} \cdot \left(1-\frac{k_q}{q}\right) \cdot \frac{C}{C+K_C \cdot X} \cdot X - \mu_d \cdot X^2 \tag{8a}$$

$$\frac{dN}{dt} = -Y_{N/X} \cdot \mu_{max} \cdot \frac{N}{N+K_N \cdot X} \cdot \frac{C}{C+K_C \cdot X} \cdot X \tag{8b}$$

$$\frac{dq}{dt} = \mu_{max} \cdot \frac{C}{C+K_C \cdot X} \cdot \left(Y_{q/X} \cdot \frac{N}{N+K_N \cdot X} - \left(1-\frac{k_q}{q}\right) \cdot q\right) \tag{8c}$$

$$\frac{dC}{dt} = -Y_{C/X} \cdot \mu_{max} \cdot \left(1-\frac{k_q}{q}\right) \cdot \frac{C}{C+K_C \cdot X} \cdot X \tag{8d}$$

$$\frac{dO}{dt} = Y_{O/X} \cdot \mu_{max} \cdot \frac{N}{N+K_N X} \cdot \frac{C}{C+K_C \cdot X} \cdot X - Y_d \cdot \mu_d \cdot X^2 \cdot f(O) \tag{8e}$$

$$\frac{dH}{dt} = \left(K_{H_2,1} \cdot \frac{dX}{dt} + K_{H_2,2} \cdot X\right) \cdot f(N) \cdot (1-f(O)) \tag{8f}$$

Overall, the challenges for the modified models are (1) how to design a model capable of accurately representing all the distinct growth periods successively, and (2) how to process the parameter estimation over 70 experimental points fitted simultaneously, given that the model that satisfies requirement (1) is highly nonlinear.

2.5. Construction of piecewise models

Piecewise models are also constructed in this study, decomposing the modified Droop model and the modified Contois model into different sub-models corresponding to different growth phases (Zhang et al., under review). The aim of discretising a model into sub-models is to avoid the challenges faced in the modified models, and by this means the parameter estimation in each sub-model therefore is easier to carry out. The challenge for the piecewise models is to fit different sub-models to the different stages of the dynamic process. Finally, the switch functions in Eq. (9) (Fig. 3), are used to combine sub-models and mediate the start and termination of each sub-model (Zhang et al., under review):

$$f(x) = 0.5 \cdot \left(1 + \frac{x-x_T}{\sqrt{(x-x_T)^2+0.01^2}}\right) \tag{9}$$

2.5.1. The piecewise Droop model

In this study, the piecewise Droop model decomposes the modified Droop model into two sub-models which correspond to cyanobacterial growth phases (including the stationary phase) and cyanobacteria decay phase, respectively. Although Eq. (1b) is widely used in the Droop model, it still lacks a theoretical explanation. Previous research Fouchard et al. (2009) has declared that it is not applicable for green algae hydrogen production simulation. Since the expression of $f(Q)$ is difficult to determine and as current experiments cannot measure nitrogen quota, $f(Q)$ has to be replaced in the piecewise Droop model.

In the cyanobacterial first growth phase, where both glycerol and nitrate are still present in excess, it assumes that the loss of nitrogen quota can be replenished rapidly by nitrate so that the first term on the right hand side of Eq. (4a) is replaced by Eq. (10) from the Monod model (Vatcheva et al., 2006). During the second growth phase where only glycerol is present, it is acceptable to use an average growth rate μ_0 to simplify the influence of the nitrogen quota on bacterial growth rate, because this phase only lasts for a short time until the nitrogen quota drops to its minimum threshold (q_T):

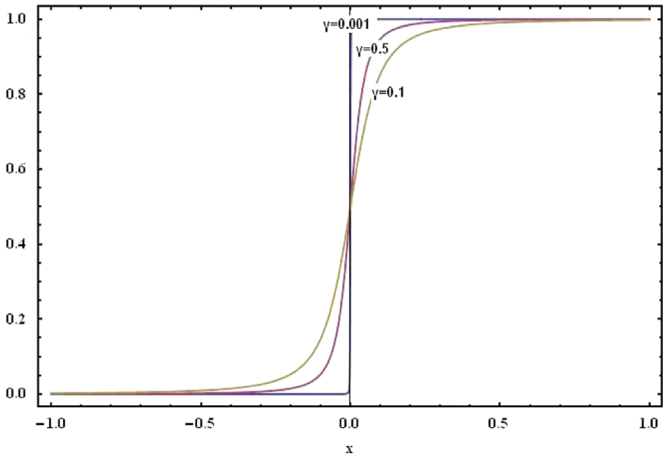

Fig. 3. Example of switch function. Eq. (9) means when $x \geq x_T$, $f(x) = 1$; otherwise $f(x) = 0$.

$$\frac{dX}{dt} = \mu_{max} \cdot \frac{N}{N+K_N} \cdot \frac{C}{C+K_C} \cdot X - \mu_d \cdot X^2 \tag{10}$$

Similarly, during the first growth phase the nitrogen quota can be simplified as constant until nitrate in the culture drops to a low concentration (N_T) which is not enough to replenish the nitrogen quota. After that the nitrogen quota starts to decrease. After the exhaustion of nitrate, the total nitrogen quota ($q \cdot X$) is a constant because there is no replenishment. Hence it is easy to calculate the consumption rate of nitrogen quota in each cell by Eq. (11). Finally, Eqs. 12(a–f) show the details of the piecewise Droop model.

$$\frac{dq}{dt} = -\frac{q}{X} \cdot \frac{dX}{dt} = -\mu_0 \cdot q \tag{11}$$

$$\frac{dX}{dt} = \begin{cases} \mu_{max} \cdot \frac{N}{N+K_N} \cdot \frac{C}{C+K_C} \cdot X + \mu_0 \cdot X - \mu_d \cdot X^2 & q > q_T \\ \mu_{max} \cdot \frac{N}{N+K_N} \cdot \frac{C}{C+K_C} \cdot X - \mu_d \cdot X^2 & q \leq q_T \end{cases} \tag{12a}$$

$$\frac{dN}{dt} = -Y_{N/X} \cdot \mu_{max} \cdot \frac{N}{N+K_N} \cdot \frac{C}{C+K_C} \cdot X \tag{12b}$$

$$\frac{dq}{dt} = \begin{cases} 0 & N > N_T \\ Y_{q/X} \cdot \mu_{max} \cdot \frac{N}{N+K_N} \cdot \frac{C}{C+K_C} - \mu_0 \cdot q & N \leq N_T \end{cases} \tag{12c}$$

$$\frac{dC}{dt} = \begin{cases} -Y_{C/X,1} \cdot \mu_{max} \cdot \frac{N}{N+K_N} \cdot \frac{C}{C+K_C} \cdot X - Y_{C/X,2} \cdot \mu_0 \cdot X & q > q_T \\ -Y_{C/X,1} \cdot \mu_{max} \cdot \frac{N}{N+K_N} \cdot \frac{C}{C+K_C} \cdot X & q \leq q_T \end{cases} \tag{12d}$$

$$\frac{dO}{dt} = Y_{O/X} \cdot \mu_{max} \cdot \frac{N}{N+K_N} \cdot \frac{C}{C+K_C} \cdot X - Y_d \cdot \mu_d \cdot X^2 \tag{12e}$$

$$\frac{dH}{dt} = K_{H_2,1} \cdot \frac{dX}{dt} + K_{H_2,2} \cdot X \tag{12f}$$

2.5.2. The piecewise Contois model

The piecewise Contois model is constructed by the same method used for the piecewise Droop model construction. Eqs. 13(a–f) show the details of the piecewise Contois model:

$$\frac{dX}{dt} = \begin{cases} \mu_{max} \cdot \frac{N}{N+K_N \cdot X} \cdot \frac{C}{C+K_C \cdot X} \cdot X + \mu_0 \cdot X - \mu_d \cdot X^2 & q > q_T \\ \mu_{max} \cdot \frac{N}{N+K_N \cdot X} \cdot \frac{C}{C+K_C \cdot X} \cdot X - \mu_d \cdot X^2 & q \leq q_T \end{cases} \tag{13a}$$

$$\frac{dN}{dt} = -Y_{N/X} \cdot \mu_{max} \cdot \frac{N}{N+K_N \cdot X} \cdot \frac{C}{C+K_C \cdot X} \cdot X \tag{13b}$$

$$\frac{dq}{dt} = \begin{cases} 0 & N > N_T \\ Y_{q/X} \cdot \mu_{max} \cdot \frac{N}{N+K_N \cdot X} \cdot \frac{C}{C+K_C \cdot X} - \mu_0 \cdot q & N \le N_T \end{cases} \tag{13c}$$

$$\frac{dC}{dt} = \begin{cases} -Y_{C/X,1} \cdot \mu_{max} \cdot \frac{N}{N+K_N \cdot X} \cdot \frac{C}{C+K_C \cdot X} \cdot X - Y_{C/X,2} \cdot \mu_0 \cdot X & q > q_T \\ -Y_{C/X,1} \cdot \mu_{max} \cdot \frac{N}{N+K_N \cdot X} \cdot \frac{C}{C+K_C \cdot X} \cdot X & q \le q_T \end{cases} \tag{13d}$$

$$\frac{dO}{dt} = Y_{O/X} \cdot \mu_{max} \cdot \frac{N}{N+K_N \cdot X} \cdot \frac{C}{C+K_C \cdot X} \cdot X - Y_d \cdot \mu_d \cdot X^2 \tag{13e}$$

$$\frac{dH}{dt} = K_{H_2,1} \cdot \frac{dX}{dt} + K_{H_2,2} \cdot X \tag{13f}$$

2.6. The parameter estimation method

In this section the mathematical method used to obtain parameters in both piecewise models is described. Once a dynamic model is designed several values for parameters need to be found. This results in a parameter estimation problem where the parameters that best fit experimental data need to be found. The parameter estimation for the dynamic model is done by setting up an optimisation problem. A general optimisation problem is defined as:

$$\min_x f(x) \tag{14a}$$

subject to

$$h(x) = 0 \tag{14b}$$

$$g(x) \le 0 \tag{14c}$$

where $x \in R^n$, $f(x) : R^n \to R$, $h(x) : R^n \to R^m$ and $g(x) : R^n \to R^r$, n is the number of variables, m is the number of equality constraints and r is the number of inequality constraints. The objective of an optimisation problem is to find the values of x, for which the minimum value of $f(x)$ is achieved such that is satisfies the constraints $h(x)$ and $g(x)$. Specific to the current optimisation function, the bounds $x \ge 0$ since x denotes the concentrations of different substrates (nitrate, oxygen, glycerol) and biomass.

To obtain the best fitting parameters, the following optimisation problem is used:

$$\min_p \sum_{i=1}^{n} \sum_{j=1}^{DP_i} (x_{ij} - d_{ij})^2 \frac{2}{\max_{i=1,2,\ldots,n}\{d_i\} + \min_{i=1,2,\ldots,n}\{d_i\}} \tag{15}$$

subject to

Kinetic and mass balance equations written in the form:

$$h(x; p) = 0$$

where n is the number of variables x for which experimental data is relevant, DP is the number of data points corresponding to variable x_i, d_{ij} is the particular data point j corresponding to variable x_i. Finally, p signifies the vector of parameters that need to be estimated for the particular model being fitted. The optimisation problem (equation number for the optimisation problem) is a weighted least squares problem, where the difference between the experimental data points, and the dynamic model is minimised. The term

$$\frac{2}{\max_{i=1,2,\ldots,n}\{d_i\} + \min_{i=1,2,\ldots,n}\{d_i\}}$$

is a weight factor included in the objective function which is unique to each variable's data points. This weight factor ensures that all variables have similar weights in the objective function, and the parameter estimation procedure finds the best possible value for the whole model rather than focusing on specific sets of variables whose magnitude is substantially greater than the others.

Several methodologies exist to optimise a model comprised of a set of Differential-Algebraic Equations (DAE). Computational experiments (Biegler, 2007) have shown that the best approach to optimise a DAE system is to fully discretise the system, transforming it into a system of nonlinear algebraic equations and then using a nonlinear optimisation code to solve the resulting optimisation problem (Biegler, 2010). This methodology was the one followed to optimise the parameters for the dynamic model. Discretisation of the DAE system is carried out through a fourth order orthogonal collocation method in this work, which is equivalent to a fourth order implicit Runge–Kutta numerical integration method. Orthogonal collocation methods are high order implicit discretization methods which provide accurate profiles with relatively few finite elements as well as good stability when solving stiff systems.

The implementation for the optimisation problems shown in this work is done in Pyomo, a Python-based optimisation environment. Specifically, Pyomo (Hart et al., 2012) is a tool package for modelling optimisation applications in Python, and is used in our work to discretise and optimise parameter estimation problems. The specific nonlinear programming problem (NLP) solver used to carry out the optimisation is IPOPT (Wächter and Biegler, 2005) (used as a library in Pyomo).

3. Results and discussion

3.1. Results of parameter estimation in kinetic models

By carrying out the optimisation method introduced above, parameters in the modified Droop model are shown in Table 1, parameters in the modified Contois model are shown in Table 2, parameters in the piecewise Droop model are shown in Table 3 and parameters in the piecewise Contois model are shown in Table 4. The values of parameters in the current models are similar with those shown in the previous publication (Alagesan et al., 2013), and the greatest value of the least-squares objective functions in the current parameter estimation process is 6.42, corresponding to the modified Contois model which parameters are determined by 70 points.

From Tables 1 to 4, it is found that the half-velocity constant of glycerol K_C is 0. This result is reasonable because only limiting nutrients can significantly affect cyanobacterial growth rate and then be simulated by kinetic models. In the current research glycerol is always available during all growth phases of cyanobacteria because it is used to provide electrons for hydrogen production. Furthermore, its existence can also facilitate the cyanobacterial O_2 consumption so that the anaerobic circumstance can be guaranteed. Hence the change of glycerol concentration is only dependent on cyanobacterial growth rate.

Another interesting result is that $K_{H_2,1}$, the hydrogen yield coefficient accounting for the influence of cyanobacterial growth rate on hydrogen production rate, is 0. It means that hydrogen production is only determined by biomass concentration in the

Table 1
Values of parameters in the Droop model.

Parameter	Value	Unit	Parameter	Value	Unit
μ_{max}	0.0485	h^{-1}	μ_d	0.0235	$L\,g^{-1}\,h^{-1}$
$Y_{q/X}$	0.6536	–	k_q	0.10	–
K_N	19.098	$mg\,L^{-1}$	K_C	0	$mg\,L^{-1}$
$Y_{C/X}$	14.049	$mmol\,g^{-1}$	$Y_{N/X}$	427.40	$mg\,g^{-1}$
$Y_{O/X}$	121.65	$L\,g^{-1}$	Y_d	403.40	$L\,g^{-1}$
$K_{H_2,1}$	0	$mL\,g^{-1}$	$K_{H_2,2}$	2.3418	$mL\,g^{-1}\,h^{-1}$

Table 2
Values of parameters in the Contois model.

Parameter	Value	Unit	Parameter	Value	Unit
μ_{max}	0.0528	h^{-1}	μ_d	0.0215	$L\,g^{-1}\,h^{-1}$
$Y_{q/X}$	0.3788	–	k_q	0.10	–
K_N	53.730	–	K_C	0	–
$Y_{C/X}$	14.049	$mmol\,g^{-1}$	$Y_{N/X}$	430.47	$mg\,g^{-1}$
$Y_{O/X}$	123.11	$L\,g^{-1}$	Y_d	440.93	$L\,g^{-1}$
$K_{H_2,1}$	0	$mL\,g^{-1}$	$K_{H_2,2}$	2.3418	$mL\,g^{-1}\,h^{-1}$

Table 3
Values of parameters in the piecewise Droop model.

Parameter	Value	Unit	Parameter	Value	Unit
μ_{max}	0.035	h^{-1}	μ_d	0.005	$L\,g^{-1}\,h^{-1}$
μ_0	0.016	h^{-1}	k_q	0.10	–
$Y_{q/X}$	0.9057	–	K_C	0	$mmol\,L^{-1}$
K_N	19.100	$mg\,L^{-1}$	$Y_{N/X}$	431.87	$mg\,g^{-1}$
$Y_{C/X,1}$	13.100	$mmol\,g^{-1}$	$Y_{C/X,2}$	32.406	$mmol\,g^{-1}$
$Y_{O/X}$	94.631	$L\,g^{-1}$	Y_d	740.60	$L\,g^{-1}$
$K_{H_2,1}$	0	$mL\,g^{-1}$	$K_{H_2,2}$	2.3418	$mL\,g^{-1}\,h^{-1}$
N_T	5.00	$mg\,L^{-1}$	q_T	0.50	–

Table 4
Values of parameters in the piecewise Contois model.

Parameter	Value	Unit	Parameter	Value	Unit
μ_{max}	0.036	h^{-1}	μ_d	0.005	$L\,g^{-1}\,h^{-1}$
μ_0	0.016	h^{-1}	k_q	0.10	–
$Y_{q/X}$	0.8806	–	K_C	0	–
K_N	50.933	$mg\,L^{-1}$	$Y_{N/X}$	430.47	$mg\,g^{-1}$
$Y_{C/X,1}$	5.2361	$mmol\,g^{-1}$	$Y_{C/X,2}$	38.656	$mmol\,g^{-1}$
$Y_{O/X}$	94.781	$L\,g^{-1}$	Y_d	740.60	$L\,g^{-1}$
$K_{H_2,1}$	0	$mL\,g^{-1}$	$K_{H_2,2}$	2.3418	$mL\,g^{-1}\,h^{-1}$
N_T	5.00	$mg\,L^{-1}$	q_T	0.55	–

culture. This may be because in cyanobacterial first growth phase hydrogen production is inhibited due to the existence of nitrate and oxygen, while in the second growth phase the growth rate is low and thus has little influence on hydrogen production rate.

3.2. Comparison of kinetic models

Once parameters in each model are calculated, it is important to verify and compare the accuracy of different kinetic models. Meanwhile it is also important to explore the stability of current models, meaning the influence of perturbation of parameters on simulation results, because the kinetic models being used in future research must possess high stability and accuracy.

To detect the accuracy of these models, the simulation results of four models are individually compared with the experimental results of the first batch experiment. Figs. 4 and 5 show the comparison of experimental results and simulation results of different models. From Fig. 4, it is found that both of the modified models can fit experimental data well in most phases except the late decay phase (after the 100th hour) and the brief initial hydrogen production period.

In the late decay phase, both of the modified models overestimate the decay rate of biomass. Compared to the modified models, the piecewise models show a better profile in the two growth phases and the stationary phase, and also more accurate results in the late decay phase. However, none of the models are capable of simulating the initial increase of hydrogen production rate, which is physically mediated by the activity of nitrogenase. As the activation of nitrogenase is controlled in a complicated way by the culture nitrate concentration and the shift from aerobic condition to anaerobic condition, switch functions are applied to simplify the real metabolic mechanism during this transitory period, and to ensure the accuracy of the simulation of hydrogen production rate in most of the other phases.

The high accuracy of piecewise models for experimental data fitting is attributed to the piecewise model construction strategy discussed before. The piecewise model construction strategy is able to punctually mediate the start and termination of each cyanobacterial growth phase. Despite the high accuracy of piecewise models, their high complexity and low flexibility may lower their accuracy if they are used to simulate a bio-production process whose operating conditions are quite different with those in the current experiment.

To further verify the accuracy of current models, all of them are used to predict the performance of a new process, the batch operation period in the second experiment, which operating condition is different with the first set of batch process. Fig. 6 shows the comparison of simulation results of our four models to experimental results. From Fig. 6, it is found that although nitrate concentration is better predicted by the two piecewise models, biomass concentration is better predicted by the two modified models. Hence, it is concluded that although the piecewise models fit better the experimental data, this does not corresponds to higher accuracy when modelling an new process.

All the models are then applied to predict the maximum biomass concentration in the culture where both nitrate and glycerol are always sufficient. Theoretically bacteria cannot keep growing even if the culture is always nutrient-sufficient as light is usually limited in highly dense cultures, and a maximum biomass concentration should exist. Previous experimental research found that the maximum cyanobacterial biomass concentration is around 40 mg Chl L^{-1} (3 g (dry weight) L^{-1}) if all nutrients are kept sufficient (Dechatiwongse et al., 2014). Fig. 7 shows simulation results of the modified Contois model and the piecewise Contois model when cyanobacteria grow in a culture with high initial glycerol and nitrate concentrations.

From Fig. 7, it is found that the piecewise Contois model shows a much higher biomass concentration in the stationary phase compared to the modified Contois model. It is easily seen that the piecewise Contois significantly overestimates 3-fold the maximum biomass concentration. The modified Contois model predicts a maximum biomass concentration of 2 g (dry weight) L^{-1} which is slightly lower than the experimental result because of the overestimated bacterial decay rate. However, this result is much more accurate compared to the piecewise Contois model.

The reason why the piecewise model has a large error is that in its construction strategy, parameters are fitted in a specific growth period without taking other periods into account. Despite the good fit in the specific growth period, large errors may be induced when simulating other processes. For example, the specific decay rate, μ_d, was fitted by the experimental data only in the cyanobacterial decay phase.

The model thereby can represent adequately the decay phase. Compared to the piecewise models, the specific decay rate in the modified models were fitted by the experimental data including the entire growth phase. The model can represent the first and second growth phases well but overestimate the decay phase as the value of μ_d is determined in all the experimental data instead of those in the decay phase. But when the models are applied to simulate a new process, the modified models can show higher accuracy as the values of their parameters are determined by the whole process, while those in the piecewise models are determined by a specific period and not being representative of other periods if the operating conditions are changed.

3.3. Sensitivity analysis of kinetic models

Finally sensitivity analysis is carries out on the different models presented in this work. A normalised sensitivity is defined by Eq. (16), which means the proportional change of y (model output) with respect the proportional change of x (model parameter). The

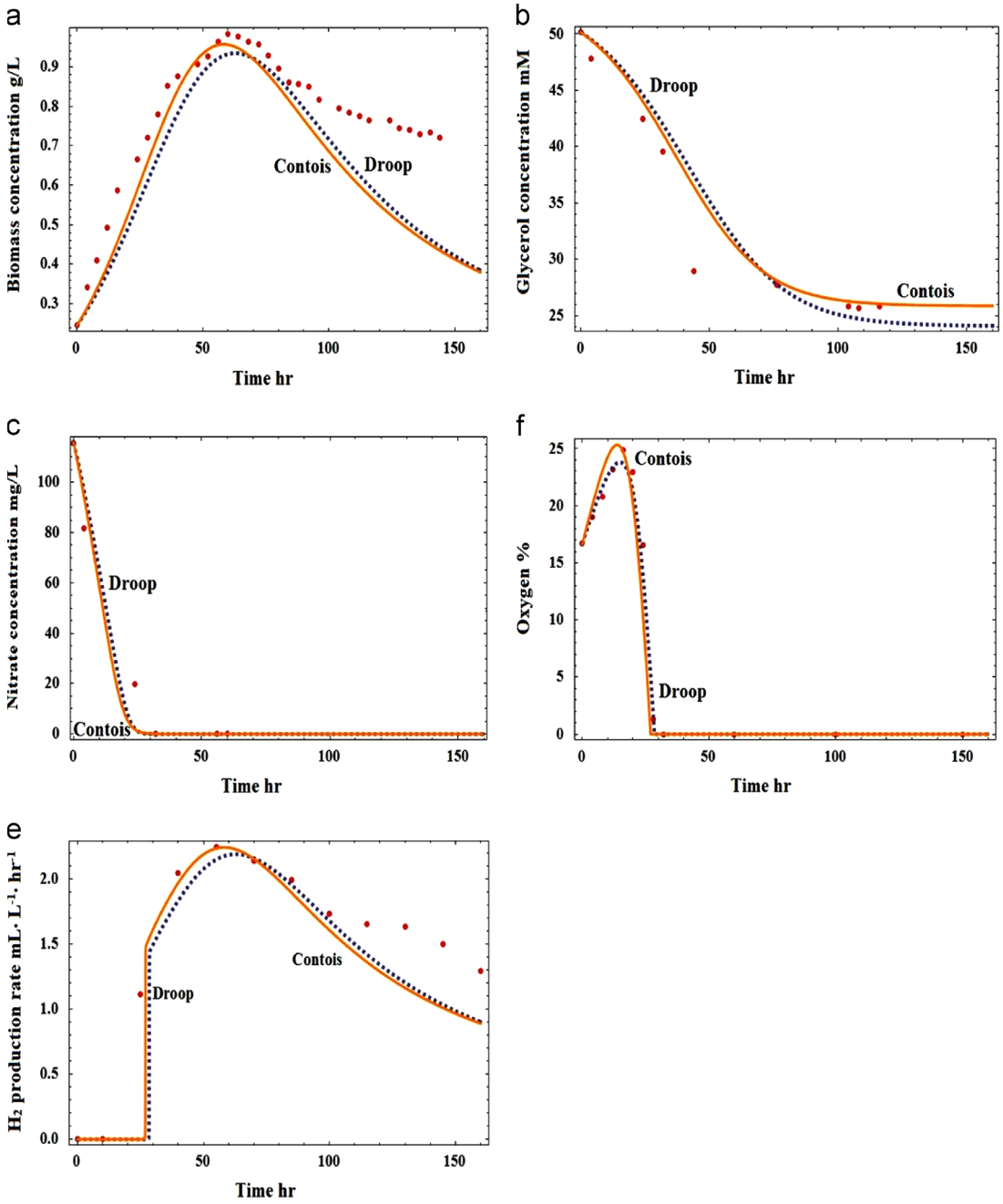

Fig. 4. Comparison of the simulation and experimental results of the first batch process experiment. Solid lines represent the simulation results of the Contois model, Dashed lines represent the simulation results of the Droop model, points are the experimental results.

definition of the normalised sensitivity in the current works have two meanings. First, for a specific parameter, the sensitivities of different model outputs with respect to this parameter directly show the significance of this parameter on different model outputs. Second, for a specific model output, the sensitivity of this model output with respect to different parameters indicates which parameter the model output is most sensitive to. Thus by conducting sensitivity analysis, it is easy to compare the significance of each parameter on different model outputs as well as the dependence of each model output on different parameters:

$$S_{y/x} = \frac{dy}{dx} \cdot \frac{x}{y} \tag{16}$$

where y is simulation result such as biomass concentration; x is parameter in the model; $S_{y/x}$ is sensitivity of y with respect to x. A positive sensitivity means the increase of y can increase x, while a negative sensitivity means increasing y leads to a decrease of x.

The sensitivities in Eq. (16) were calculated through a dedicated DAE simulation package written in *Mathematica*[M], which automatically processes symbolically a DAE model and augments it by the associated parametric sensitivity equations required (Navarro and Vassiliadis, 2014).

In a kinetic model each parameter has its specific biological meaning, and its change may lead to a significant change of product yield (Klipp et al., 2005; Fouchard et al., 2009). By exploring sensitivity analysis, crucial factors affecting fermentation targets can be found, which can be used to direct the cultivation of new mutants. Furthermore, a high value of sensitivity also indicates that the value of the associated parameter should be calculated more accurately. Since the piecewise models are found to be insufficiently accurate compared to the modified models, in this section only the sensitivity of modified models is studied.

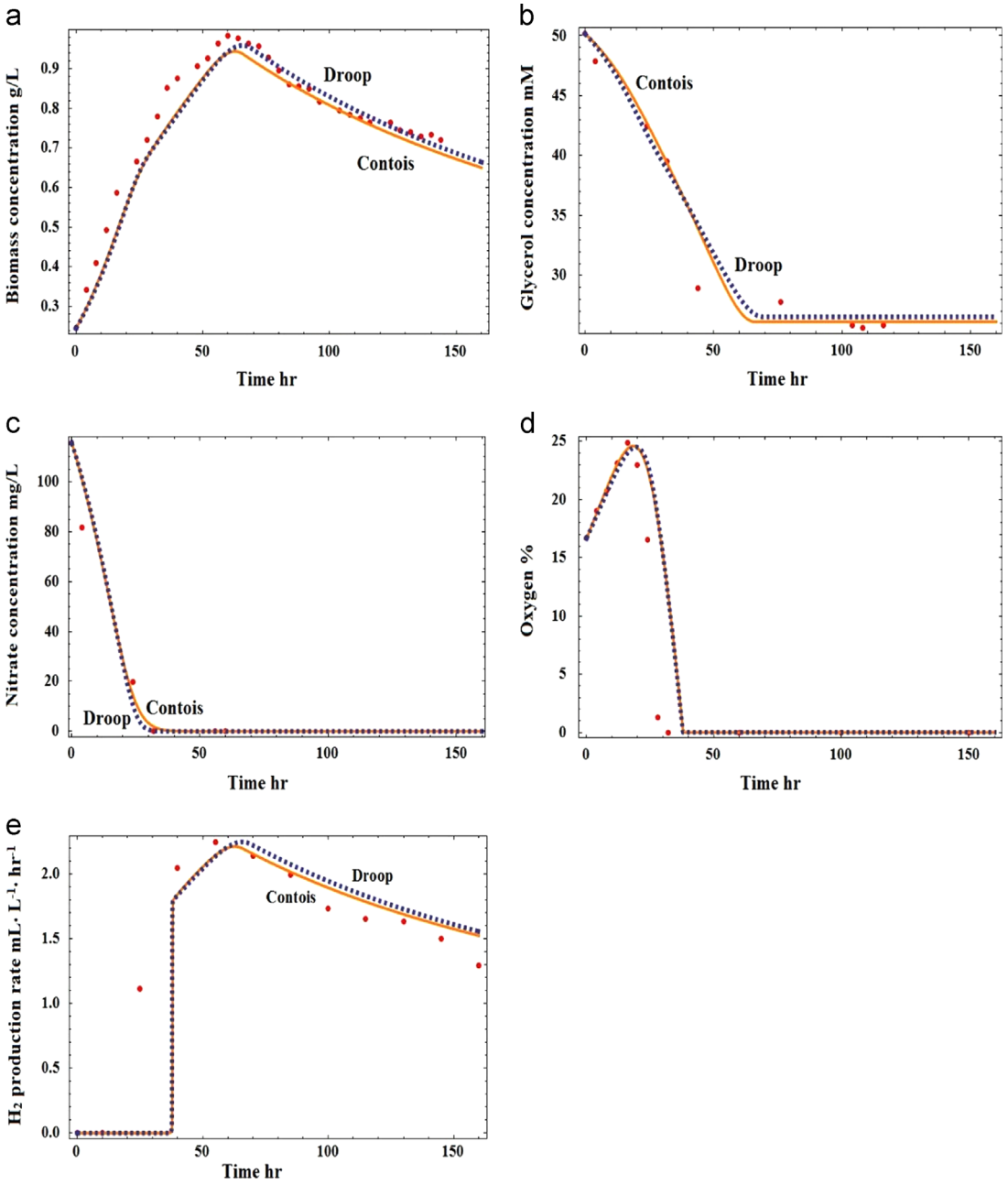

Fig. 5. Comparison of the simulation and experimental results of the first batch mode experiment. Solid lines represent the simulation results of the piecewise Contois model, Dashed lines represent the simulation results of the piecewise Droop model, points are the experimental results.

In the current research, the model outputs include hydrogen production, biomass concentration, nitrate concentration, glycerol concentration and nitrogen quota, while the model parameters are all the parameters in the modified models. Sensitivity of each dynamic variable with respect to the parameters in both modified models is calculated. Figs. 8 and 9 show the sensitivity analysis of the modified Contois model and the modified Droop model, respectively.

From Figs. 8 and 9, it is concluded that the sensitivities in both models are quite similar. Sensitivity of dynamic variables with respect to model parameters can be divided into two classes. The first class corresponds to a sensitivity lower than ± 1.0, which means a 1% change of parameter can only lead to a small change (less than 1%) on the dynamic variable. This sensitivity indicates that the dynamic variable is not sensitive to the change of the parameter. Dynamic variables which belong to this class are glycerol concentration (the greatest sensitivity with respect to parameters is less than ± 0.01), hydrogen production (the greatest sensitivity with respect to parameters is less than ± 0.01) and nitrate concentration (the greatest sensitivity with respect to parameters is less than ± 0.5). The second class refers to a sensitivity higher than (± 1.0), which indicates that the change of the parameter can lead to a larger proportional change on the dynamic variable. This sensitivity shows that the dynamic variable is highly dependent on the parameter. Dynamic variables such as nitrogen quota (the sensitivity with respect to μ_{max} is -1.6), biomass concentration (the sensitivity with respect to μ_{max} is 1.1) and oxygen concentration (the sensitivity with respect to $Y_{O/X}$ is 2.6) belong to this class.

The simulation result of oxygen concentration shows that it is mainly influenced by $Y_{O/X}$, especially when oxygen concentration is low. For example, a 1% increase of $Y_{O/X}$ leads to a 2.2% increase of oxygen concentration when oxygen is being consumed. The accuracy of μ_{max}, μ_d and k_q is important to biomass and nitrogen quota concentration. For instance, μ_{max} dominates biomass and nitrogen quota concentration during the cyanobacterial first growth phase, while the influence of k_q and μ_d becomes crucial in the

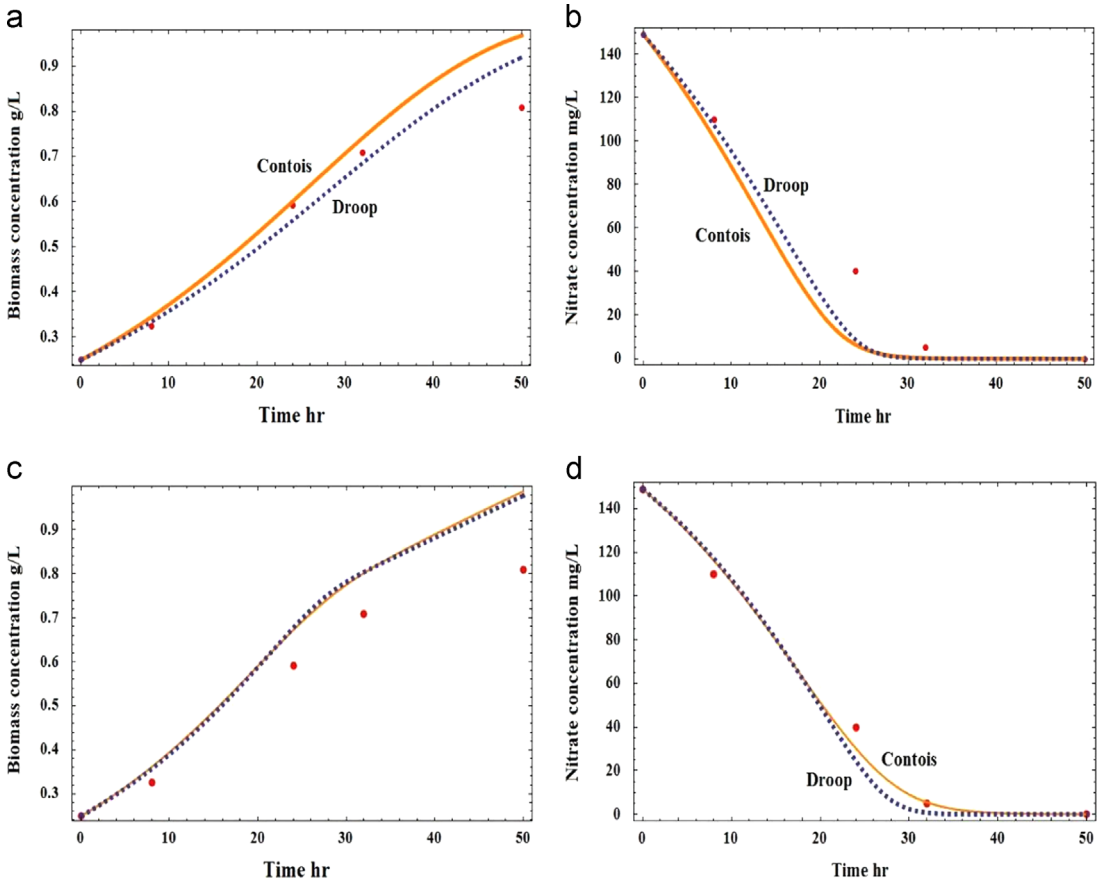

Fig. 6. Comparison of the simulation and experimental results of the second batch mode experiment. (a) Results of biomass concentration, solid line: the modified Contois model; dashed line: the modified Droop model. (b) Results of nitrate concentration. solid line: the modified Contois model; dashed line: the modified Droop model. (c) Results of biomass concentration, solid line: the piecewise Contois model; dashed line: the piecewise Droop model. (d) Results of nitrate concentration. solid line: the piecewise Contois model; dashed line: the piecewise Droop model. Red points are experimental results. (For interpretation of the references to color in this figure caption, the reader is referred to the web version of this article.)

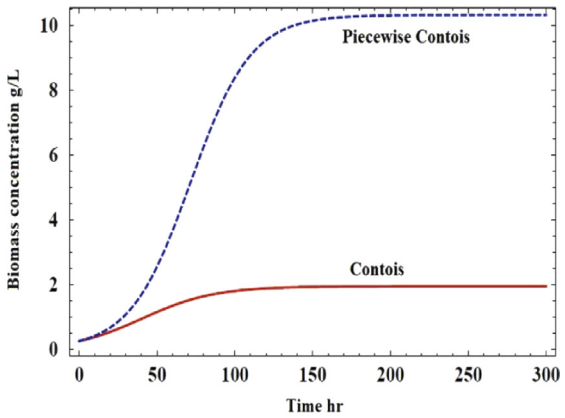

Fig. 7. Simulation results of the piecewise Contois model and the modified Contois model when both nitrate and glycerol are always in excess in the culture.

cyanobacterial stationary phase and decay phase. K_N and $Y_{N/X}$ only show small effects on nitrate concentration when nitrate is being consumed.

Overall it is concluded that in the present study most of the dynamic variables are not sensitive to the change of parameters. To enhance biomass concentration and hydrogen production, μ_{max} should be increased while both μ_d and k_q should be decreased. To facilitate the start of anaerobic conditions, $Y_{O/X}$ should be decreased. Additionally, the value of these parameters should also be verified in future research as it significantly affects the accuracy of current models. Finally by comparing the performance of different models, the present research finds that both the modified Droop model and the modified Contois model have high accuracy and can be used for further work. The drawbacks of piecewise models restrict their further application and thus they are not suitable for further research.

3.4. Simulation of continuous photoproduction process

In the present continuous photoproduction experiment, fresh cyanobacteria and nutrients including glycerol and nitrate are continuously pumped into the flat plate photobioreactor (PBR) after the 75th hour when the process operation was started. The operating conditions and experimental results are listed in Table 5.

In the current flat plate PBR, recycling gas is used to prevent the aggregation of cyanobacteria and enhance the distribution of biomass and nutrients, while the gas recycling rate is not high due to two main limitations (Zhang et al., 2015). The first limitation is that fluid stress led by high recycling rate will be intense enough to break cyanobacteria. The second limitation is that bubble volume concentration increases with the increasing recycling gas, and it can significantly enhance the reflection of light passing through the PBR. As a result, no enough light can be absorbed by cyanobacteria for their growth and hydrogen production. Therefore, the present study revised both the modified Droop model and the modified Contois model for continuous photoproduction process simulation. Two types of kinetic models are built with the assumption that the PBR is operated as CSTR or PFR, respectively. This is because it is unclear if the recycling gas rate is high enough to keep a uniform distribution of biomass and nutrients in the current PBR.

For a CSTR type reactor, the culture inside the reactor is well mixed. Eqs. 17(a–f) show the revised modified Droop model for the dynamic CSTR photoproduction process. A dynamic PFR

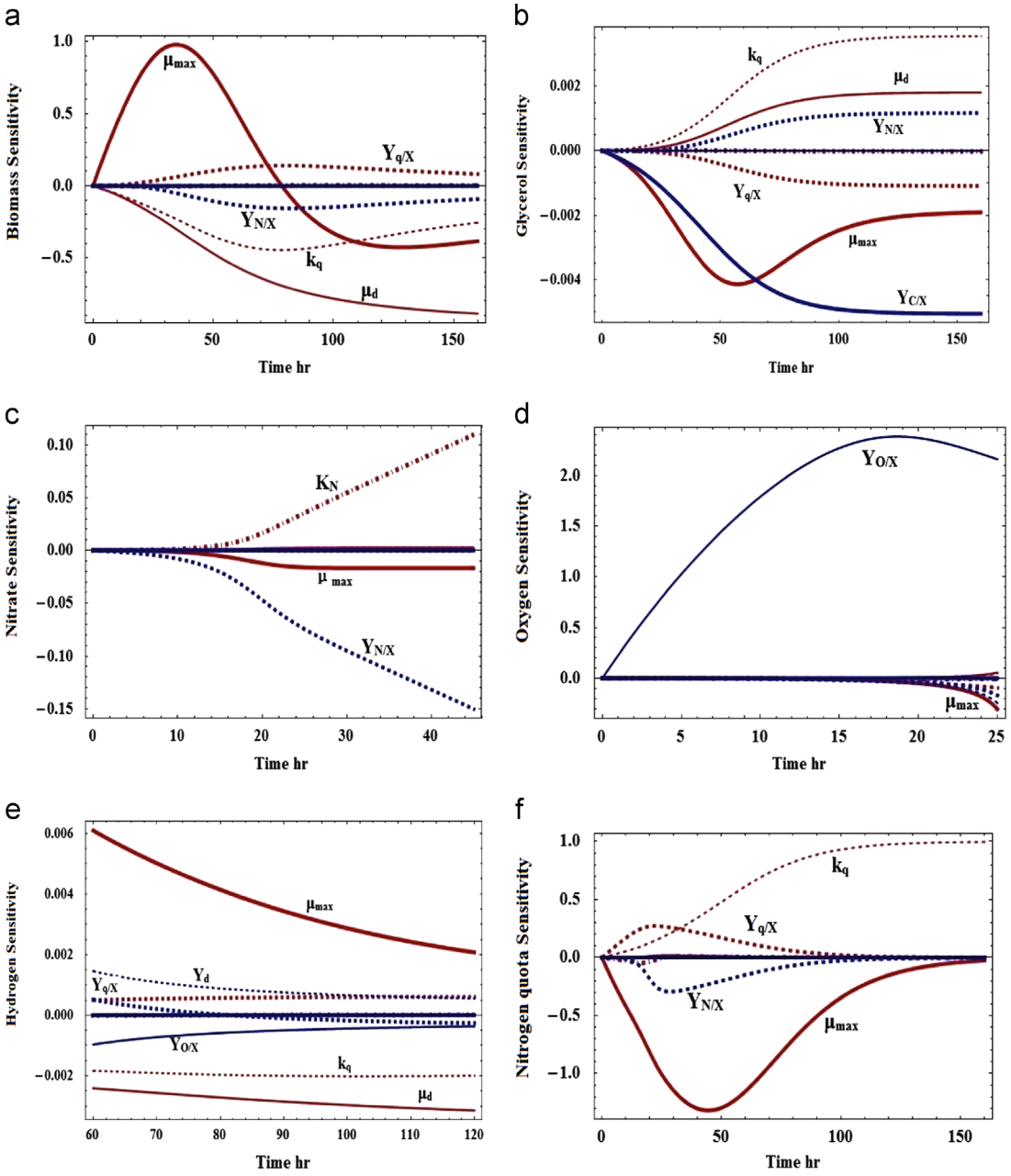

Fig. 8. Sensitivity analysis of the modified Contois model. (a) Sensitivity of biomass w.r.t. parameters in the modified Contois model; (b) sensitivity of glycerol w.r.t. parameters in the modified Contois model; (c) sensitivity of nitrate w.r.t. parameters in the modified Contois model; (d) sensitivity of oxygen w.r.t. parameters in the modified Contois model; (e) sensitivity of hydrogen w.r.t. parameters in the modified Contois model; and (f) sensitivity of nitrogen quota w.r.t. parameters in the modified Contois model. Sensitivity analysis was only conducted when the substrate or biomass existed in the culture. Specific to hydrogen, the final time was chosen as the 120th hour beyond which a significant decrease of biomass concentration and hydrogen production rate was found.

photoproduction process is much more complicated. Because the concentration of biomass and nutrients changes along culture movement direction and operation time, kinetic models have to be revised to partial differential equations. To simplify the dynamic PFR model, only the performance of PFR photoproduction process under steady state is analysed. Eqs. 18(a–f) show the PFR steady state model:

$$\frac{dX}{dt}=\mu_{max}\cdot\left(1-\frac{k_q}{q}\right)\cdot\frac{C}{C+K_C}\cdot X-\mu_d\cdot X^2+Di\cdot(X_1-X) \tag{17a}$$

$$\frac{dN}{dt}=-Y_{N/X}\cdot\mu_{max}\cdot\frac{N}{N+K_N}\cdot\frac{C}{C+K_C}\cdot X+Di\cdot(N_1-N) \tag{17b}$$

$$\frac{dq}{dt}=\mu_{max}\cdot\frac{C}{C+K_C}\cdot\left(Y_{q/X}\cdot\frac{N}{N+K_N}-\left(1-\frac{k_q}{q}\right)\cdot q\right)+Di\cdot(q_1-q) \tag{17c}$$

$$\frac{dC}{dt}=-Y_{C/X}\cdot\mu_{max}\cdot\left(1-\frac{k_q}{q}\right)\cdot\frac{C}{C+K_C}\cdot X+Di\cdot(C_1-C) \tag{17d}$$

$$\frac{dO}{dt}=Y_{O/X}\cdot\mu_{max}\cdot\frac{N}{N+K_N}\cdot\frac{C}{C+K_C}\cdot X-Y_d\cdot\mu_d\cdot X^2\cdot f(O)+Di\cdot(O_1-O) \tag{17e}$$

$$\frac{dH}{dt}=\left(K_{H_2,1}\cdot\frac{dX}{dt}+K_{H_2,2}\cdot X\right)\cdot f(N)\cdot(1-f(O)) \tag{17f}$$

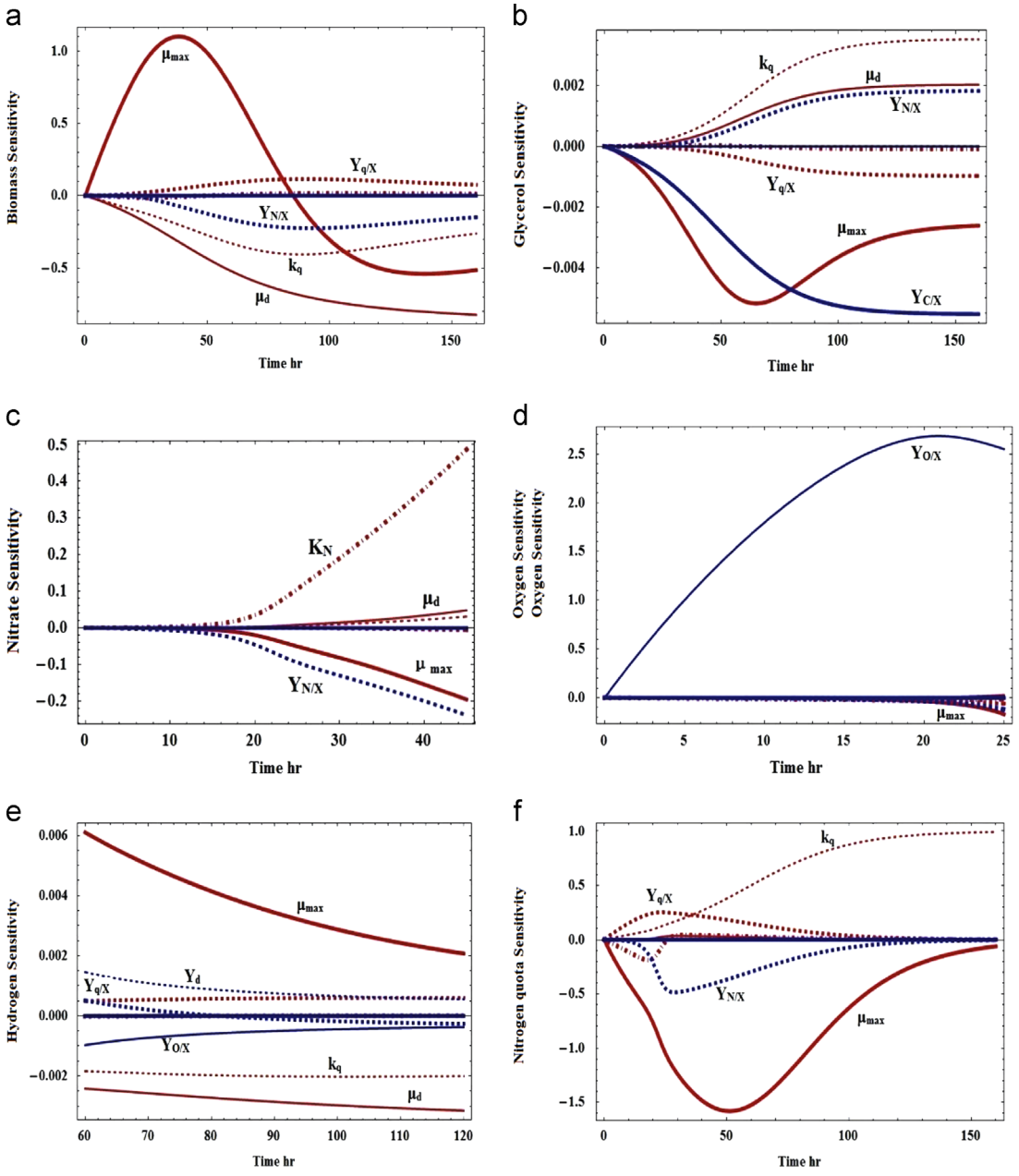

Fig. 9. Sensitivity analysis of the modified Droop model. (a) Sensitivity of biomass w.r.t. parameters in the modified Droop model; (b) sensitivity of glycerol w.r.t. parameters in the modified Droop model; (c) sensitivity of nitrate w.r.t. parameters in the modified Droop model; (d) sensitivity of oxygen w.r.t. parameters in the modified Droop model; (e) sensitivity of hydrogen w.r.t. parameters in the modified Droop model; (f) sensitivity of nitrogen quota w.r.t. parameters in the modified Droop model. Sensitivity analysis was only conducted when the substrate or biomass existed in the culture. Specific to hydrogen, the final time was chosen as the 120th hour beyond which a significant decrease of biomass concentration and hydrogen production rate was found.

Table 5
Operating conditions and results of the continuous photoproduction process.

Initial O_2	0.0%	Initial biomass	0.8 g L^{-1}	Initial nitrate	0.0 mg L^{-1}
Initial glycerol	30 mM	Initial hydrogen	0.0 mL	Influent O_2	30%[a]
Influent biomass	2.0 g L^{-1}	Influent nitrate	1470 mg L^{-1}	Influent glycerol	Sufficient
Effluent O_2	0.0%	Effluent biomass	1.5 g L^{-1}	Effluent nitrate	0.0 mg L^{-1}
Effluent glycerol	30 mM	Total hydrogen	1750 mL	Dilution rate	0.015 h^{-1}
Operation time	750 h	Reactor length	0.2 m	Reactor volume	1 L

[a] The influent oxygen concentration eventually drops to 0% because of the consumption by cyanobacteria in the tubular photobioreactor. Initial concentration of nutrients listed in the table is at the beginning of continuous operation, instead of the beginning of batch operation.

In the current research, hydrogen is captured from the top of the PBR instead of the effluent culture. Because hydrogen production rate is only dependent on the biomass concentration and independent of the removal method, it is acceptable to assume that hydrogen is trapped in the reactor permanently in both the CSTR process and the PFR process. Specific to the PFR process where steady state is assumed, hydrogen production has to be changed to hydrogen production rate (H_r, mL L^{-1} h^{-1}) which is a

constant at steady state. The derivation of Eq. (19) is shown below:

$$\frac{dX}{dl} = \left[\mu_{max} \cdot \left(1 - \frac{k_q}{q}\right) \cdot \frac{C}{C+K_C} \cdot X - \mu_d \cdot X^2\right] / (Di \cdot L) \quad (18a)$$

$$\frac{dN}{dl} = \left[-Y_{N/X} \cdot \mu_{max} \cdot \frac{N}{N+K_N} \cdot \frac{C}{C+K_C} \cdot X\right] / (Di \cdot L) \quad (18b)$$

$$\frac{dq}{dl} = \left[\mu_{max} \cdot \frac{C}{C+K_C} \cdot \left(Y_{q/X} \cdot \frac{N}{N+K_N} - \left(1 - \frac{k_q}{q}\right) \cdot q\right)\right] / (Di \cdot L) \quad (18c)$$

$$\frac{dC}{dl} = \left[-Y_{C/X} \cdot \mu_{max} \cdot \left(1 - \frac{k_q}{q}\right) \cdot \frac{C}{C+K_C} \cdot X\right] / (Di \cdot L) \quad (18d)$$

$$\frac{dO}{dl} = \left[\frac{Y_{O/X} \cdot \mu_{max} \cdot N}{N+K_N} \cdot \frac{C}{C+K_C} \cdot X - Y_d \cdot \mu_d \cdot X^2 \cdot f(O)\right] / (Di \cdot L) \quad (18e)$$

$$\frac{dH_r}{dl} = \left[\left(K_{H_2,1} \cdot \frac{dX}{dt} + K_{H_2,2} \cdot X\right) \cdot f(N) \cdot (1 - f(O))\right] / L \quad (18f)$$

$$H_r = \int_0^L \frac{\left(K_{H_2,1} \cdot \frac{dX}{dt} + K_{H_2,2} \cdot X\right) \cdot A \cdot f(N) \cdot (1 - f(O)) \cdot dl}{L \cdot A} \quad (19)$$

where A is cross-section area of PBR perpendicular to culture movement direction, L is length of PBR along culture movement direction.

Table 6 shows the simulation results of dynamic CSTR photoproduction process and steady state PFR photoproduction process of different modified models. It is found that the simulation results of the modified Droop model and the modified Contois model are similar. By comparing the simulation and experimental results of total hydrogen production, it is indicated that the flat plate PBR is not well mixed because of the low gas recycling rate, as the hydrogen production measured from the experiment is between that from the CSTR and the PFR. The experimental results of effluent biomass concentration and effluent nitrate concentration further indicates that the current PBR is operated more similarly to a PFR since the experimental results are closer to the PFR results.

From Table 6, it is also found that the CSTR operation has higher effluent biomass concentration and hydrogen yield (production) compared to the PFR operation. Generally, PFR operation is known to have higher product yield and reactant conversion efficiency compared to CSTR operation while it cannot guarantee a higher product yield compared to CSTR if the product is an intermediate. In the current research, because cyanobacteria grow when nitrate is present and then decay after the consumption of nitrate, biomass can be regarded as an intermediate in the current photoproduction process. As hydrogen production rate is proportional to biomass concentration (Eq. (4f)), a PFR is not guaranteed to provide a higher hydrogen production rate compared to a CSTR.

Another potential reason is that hydrogen can only be produced at the place where both nitrate concentration and oxygen concentration are lower than their threshold. In a CSTR the concentration of oxygen and nitrate is uniform and can be maintained lower than the threshold. Hence hydrogen is produced in the whole range of the reactor. However, as the concentration of nitrate and oxygen decreases along the direction of culture movement in a PFR, only part of the reactor contains low oxygen and nitrate concentration and can produce hydrogen (Fig. 10). As a result, a CSTR is possible to have a higher hydrogen production rate compared to a PFR in the current operating conditions. However once the operating conditions are changed, it is still uncertain if a PFR will have a better performance compared to a CSTR.

3.5. Fixed volume fed-batch process design

The present experimental research has explored the capacity of both batch and continuous operation processes. Although it has confirmed that the continuous operation process has much higher hydrogen yield compared to the batch process, the incompatible cyanobacterial growth phase (with sufficient nitrate) and hydrogen production phase (nitrate concentration lower than 100 mg/L) lead to the continuous photoproduction process executed by connecting two reactors (one for cell growth and the other for hydrogen production) (Dechatiwongse et al., 2015). To facilitate single PBR hydrogen production photoproduction process, two kinds of fed-batch processes, a fixed volume process and a variable volume process are studied in the present simulation study.

For a fixed volume fed-batch process, the influent flow rate is constant and low so that the total volume of influent is negligible. To provide enough nutrients for cyanobacterial growth and hydrogen production, nutrients in the influent are always highly concentrated. In the current work, the design variables of the fixed volume fed-batch process are the switch time from batch operation to fed-batch operation, the influent flow rate and the influent nitrate concentration. The glycerol influent concentration is not chosen as the design variable since its concentration has to be in excess during the whole process.

At the beginning of the process, the photobioreactor is operated as the batch system same to the current experiment. Since the current experiment found that a sharp decline of the hydrogen production rate and biomass concentration starts around the 150th hour, this time is chosen as the switch time and the influent is continuously added to the reactor from that point onwards. To ensure the total feed volume is negligible (for example, less than 0.1 L) , the feeding rate has to be lower than 0.00016 L h^{-1} so that at the end of operation the culture volume is less than 1 L. To enhance hydrogen production and biomass concentration, the feed contains concentrated nitrate (1.61 mol L^{-1}) so that the culture can have sufficient nitrate for cyanobacteria growth.

Table 6
Simulation results of continuous photoproduction process.

Reactor	Model	Biomass (g L^{-1})[a]	Nitrate (mg L^{-1})[a]	Hydrogen (mL)	O_2(%)
PFR	Modified Contois	1.664	0.00	1365	0.00
	Modified Droop	1.632	0.00	1284	0.00
CSTR	Modified Contois	1.924	92.6	2334	0.01
	Modified Droop	1.795	26.6	2144	0.01
Experimental results		1.5	0.0	1750	0.0

[a] Biomass concentration and nitrate concentration represent the effluent concentration.

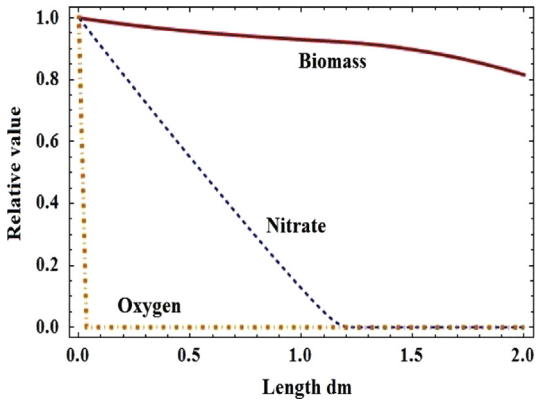

Fig. 10. Relative concentration of biomass, nitrate and oxygen along the length of PBR in steady state PFR photoproduction process. The relative concentration is defined as x/x_{max}, where x refers to the concentration of any substrates or biomass.

Table 7
Operating conditions of fixed volume fed-batch process.

Initial biomass concentration	0.2 g L^{-1}	Initial oxygen concentration	20%
Initial nitrate concentration	150 mg L^{-1}	Influent biomass concentration	0.0 g L^{-1}
Influent oxygen concentration	90%	Influent nitrate concentration	100 g L^{-1}
Feeding rate	0.00016 L h^{-1}	Glycerol concentration	Sufficient
Operation time	750 h	Switch time	150th hour

Table 7 shows the operating conditions of the fixed volume fed-batch process designed in the current research.

3.5.1. Kinetic model for fixed volume fed-batch process simulation

For a fed-batch process the reactor is usually designed similar to a CSTR, because at the beginning period the photoproduction process is operated as a batch system and the culture is well mixed. Additionally, the reactor in a fed-batch photoproduction process can rarely be designed as PFR without the provision of fresh biomass, otherwise all of the biomass in the reactor will be flushed away. The current study thereby assumes that the PBR in fed-batch photoproduction process is operated as a CSTR (thus gas recycling rate has to be increased). Because of the high similarity of both modified models, only the modified Droop model is used in this section for process simulation. Eqs. 20(a–f) show the revised modified Droop model for fixed volume fed-batch process:

$$\frac{dX}{dt}=\mu_{max}\cdot\left(1-\frac{k_q}{q}\right)\cdot\frac{C}{C+K_C}\cdot X-\mu_d\cdot X^2 \tag{20a}$$

$$\frac{dN}{dt}=-Y_{N/X}\cdot\mu_{max}\cdot\frac{N}{N+K_N}\cdot\frac{C}{C+K_C}\cdot X+F\cdot N_1 \tag{20b}$$

$$\frac{dq}{dt}=Y_{q/X}\cdot\mu_{max}\cdot\frac{N}{N+K_N}\cdot\frac{C}{C+K_C}-\mu_{max}\cdot\left(1-\frac{k_q}{q}\right)\cdot\frac{C}{C+K_C}\cdot q \tag{20c}$$

$$\frac{dC}{dt}=-Y_{C/X}\cdot\mu_{max}\cdot\left(1-\frac{k_q}{q}\right)\cdot\frac{C}{C+K_C}\cdot X+F\cdot C_1 \tag{20d}$$

$$\frac{dO}{dt}=Y_{O/X}\cdot\mu_{max}\cdot\frac{N}{N+K_N}\cdot\frac{C}{C+K_C}\cdot X-Y_d\cdot\mu_d\cdot X^2\cdot f(O)+F\cdot O_1 \tag{20e}$$

$$\frac{dH}{dt}=\left(K_{H_2,1}\cdot\frac{dX}{dt}+K_{H_2,2}\cdot X\right)\cdot f(N)\cdot(1-f(O)) \tag{20f}$$

Eq. (9) is used to control the start of feed addition.

3.5.2. Results of fixed volume fed-batch photoproduction process simulation

Fig. 11 shows the simulation results of fixed volume fed-batch process. From Fig. 11, it is concluded that at the beginning of feed initiation, there is a significant increase of nitrate concentration as well as a slight increase of oxygen concentration. Because of the replenishment, biomass concentration increases and even exceeds the highest biomass concentration during batch operation. Following that, nitrate is always present in the culture and its concentration is controlled lower than 50 mg L^{-1}. Oxygen is rapidly consumed by biomass due to the high biomass density and anaerobic condition is maintained.

On the contrary, during the first period of feed addition, hydrogen production rate declines to zero because of the inhibition of nitrate and oxygen on nitrogenase activity. After nitrate concentration drops lower than its threshold and oxygen depletion, nitrogenase activity is recovered and hydrogen production rate is significantly increased compared to the batch system. This is mainly due to the increasing biomass concentration. At the end of the process, total hydrogen production is 1560 mL L^{-1}.

3.6. Variable volume fed-batch process design

For a variable volume fed-batch process the volume of the medium in the photobioreactor varies with time because of the feed addition, thus the photobioreactor cannot be fully loaded at first. In the present design, it is assumed that the initial culture volume in the PBR is 0.5 L (half capacity) and the switch time is also at the 150th hour. The feeding rate is set as 0.0008 L h^{-1} so that the reactor is filled at the end of process. Because of the significant volume of influent, nutrients in the influent are not as concentrated as those in the fixed volume fed-batch process. The nitrate concentration in this case is calculated as 0.16 mol L^{-1} (10 g L^{-1}), and oxygen concentration is also set as 90% saturation. To ensure the same mass of cyanobacteria for hydrogen production, the initial biomass concentration in this process is set as 0.4 g L^{-1}. Table 8 shows the operating conditions of variable volume fed-batch process designed in the current research.

3.6.1. Kinetic model for variable volume fed-batch process simulation

Eqs. 21(a–g) show the revised modified Droop model for variable volume fed-batch process:

$$\frac{dX}{dt}=\left(\mu_{max}\cdot\left(1-\frac{k_q}{q}\right)\cdot\frac{C}{C+K_C}\cdot X\cdot V-\mu_d\cdot X^2\cdot V-F\cdot X\right)/V \tag{21a}$$

$$\frac{dN}{dt}=\left(-Y_{N/X}\cdot\mu_{max}\cdot\frac{N}{N+K_N}\cdot\frac{C}{C+K_C}\cdot X\cdot V+F\cdot(N_1-N)\right)/V \tag{21b}$$

$$\frac{dq}{dt}=Y_{q/X}\cdot\mu_{max}\cdot\frac{N}{N+K_N}\cdot\frac{C}{C+K_C}-\mu_{max}\cdot\left(1-\frac{k_q}{q}\right)\cdot\frac{C}{C+K_C}\cdot q \tag{21c}$$

$$\frac{dC}{dt}=\left(-Y_{C/X}\cdot\mu_{max}\cdot\left(1-\frac{k_q}{q}\right)\cdot\frac{C}{C+K_C}\cdot X\cdot V+F\cdot(C_1-C)\right)/V \tag{21d}$$

$$\frac{dO}{dt}=\frac{Y_{O/X}\cdot\mu_{max}\cdot N}{N+K_N}\cdot\frac{C}{C+K_C}\cdot X-Y_d\cdot\mu_d\cdot X^2\cdot f(O)+\frac{F}{V}\cdot(O_1-O) \tag{21e}$$

$$\frac{dH}{dt}=\left(K_{H_2,1}\cdot\frac{dX}{dt}+K_{H_2,2}\cdot X\right)\cdot f(N)\cdot(1-f(O)) \tag{21f}$$

$$\frac{dV}{dt}=F \tag{21g}$$

Similar with the fixed volume fed-batch process model, Eq. (9) is used to control the start of feed addition.

3.6.2. Results of fed-batch photoproduction process simulation

Fig. 12 shows the simulation results of variable volume fed-batch process. From Fig. 12, it is concluded that the performance of the variable volume fed-batch process is similar with the fixed volume fed-batch process. However oxygen concentration in the culture at the beginning of feed addition is much higher than that in the fixed volume fed-batch process. This increase does not influence much the hydrogen production because the high respiration rate of cyanobacteria rapidly consumes the influent oxygen.

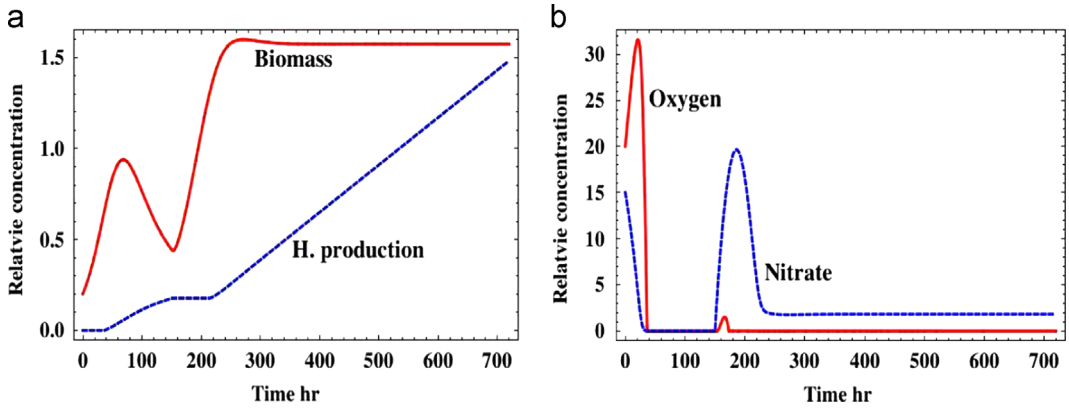

Fig. 11. Simulation results of the fixed volume fed-batch process. (a) Biomass concentration ($\times 1$g L^{-1}) and hydrogen production ($\times 1000$ mL L^{-1}); (b) oxygen concentration ($\times 1\%$) and nitrate concentration ($\times 10$mg L^{-1}).

Table 8
Operating conditions of variable volume fed-batch process.

Initial biomass concentration	0.4 g L^{-1}	Initial oxygen concentration	20%
Initial nitrate concentration	150 mg L^{-1}	Influent biomass concentration	0.0 g L^{-1}
Influent oxygen concentration	90%	Influent nitrate concentration	10.0 g L^{-1}
Feeding rate	0.0008 L h^{-1}	Glycerol concentration	Sufficient
Operation time	750 h	Switch time	150th hour

Another difference between the two processes is that in the variable volume fed-batch process, biomass concentration slightly decreases with time after operation switch. The decrease of biomass concentration is mainly because cyanobacterial growth rate is not high enough to offset the dilution by the feed. As a result, hydrogen production rate in this process also slightly decreases with time. The total hydrogen production in this process is 1529 mL L^{-1}.

3.7. Comparison of hydrogen production in different process

From Table 9, it is found that the total hydrogen production of both fed-batch photoproduction processes are higher than in the batch process, but only 87% of the continuous photoproduction process even though biomass concentration in these processes is similar. This is probably due to the brief nitrogenase inactivation period in both fed-batch processes at the start of feed addition. However a fed-batch photoproduction process only needs one PBR and its dilution rate is lower than that in the continuous process, thus both equipment investment and electricity costs can be reduced.

4. Conclusions and future research

The present study set up two modified models and two piecewise models, based on the Droop and the Contois models, to simulate different cell growth phases in cyanobacterium (*Cyanothece* sp. ATCC 51142) biohydrogen photoproduction process. Parameters in each model have been estimated via a collocation optimisation method using the full dynamic models directly. By comparing the experimental and simulation results, it is concluded that the piecewise models present a better fitting to experimental measurements compared to the modified models. The modified models can accurately simulate most of cyanobacterial growth phases except the late decay phase and the initial hydrogen production period. However, when the models are applied to simulate a new process, the modified models may show higher accuracy compared to the piecewise models.

The present research simulated the two-stage continuous photoproduction process designed in the current experiment. Because of the high influent biomass and nutrient concentration, low gas recycling and culture dilution rate, it is proposed that the current PBR is not well mixed in the current experimental work. The current research then simulates the continuous process with the assumption that the PBR is operated either as PFR or as CSTR. By comparing the experimental and simulation results, it is concluded that the current PBR is more similar to a PFR, and supported the hypothesis that the PBR is not well mixed.

It is found that a PFR has lower effluent biomass concentration and total hydrogen production compared to a CSTR in the current experimental operating conditions based on the current simulation, although a PFR is generally known to show higher product yield and reactant conversion efficiency. By analysing the simulation results, the current study proposes two potential reasons to explain this observation. The first reason is that hydrogen production rate is proportional to biomass concentration whose behaviour is quite similar to an intermediate, and thus a PFR cannot produce a higher product yield. The second reason is that hydrogen can be only generated in the volume where both oxygen and nitrate are low in a PFR, and the total volume of a PFR is thereby not well utilised under the current operating conditions. Nonetheless, it should be emphasised that once the operating conditions are changed, a PFR has the potential of better performance compared to a CSTR, and further experiments should be conducted to compare the performance of PFR and CSTR to verify the accuracy of the current work.

The current research finally presents the simulation of two fed-batch photoproduction processes to explore the feasibility of a single PBR continuous photoproduction process. From the comparison of simulation and experimental results, it is found that the total hydrogen produced in a fed-batch photoproduction process is 87% of a continuous process, while its capital cost expected to be lower as one reactor vessel is required for this process. Because light intensity and PBR configuration are vital to cyanobacterial growth and hydrogen production, future work will include these aspects so as to obtain optimised configurations in tandem with the optimisation of operating conditions for the reactors proposed.

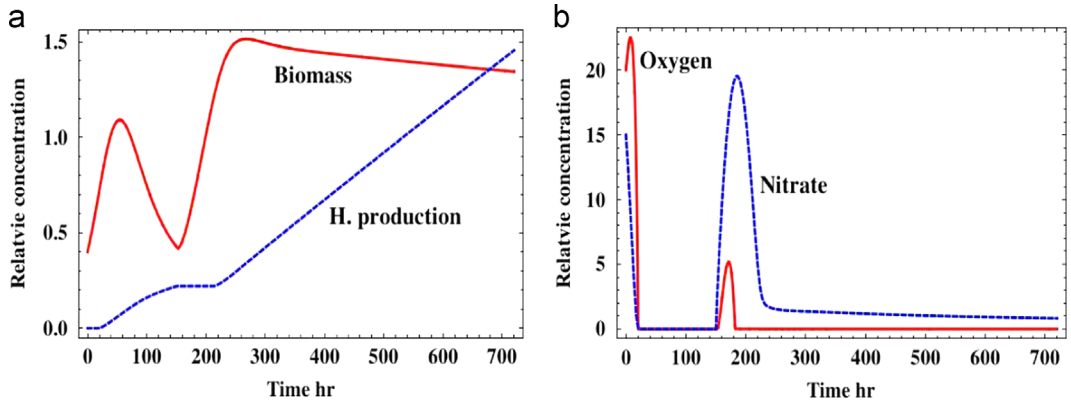

Fig. 12. Simulation results of the variable volume fed-batch process. (a) Biomass concentration ($\times 1\ g\ L^{-1}$) and hydrogen production ($\times 1000\ mL\ L^{-1}$); (b) oxygen concentration ($\times 1\%$) and nitrate concentration ($\times 10\ mg\ L^{-1}$).

Table 9
Comparison of the performance of different process.

Different process	Maximum biomass ($g\ L^{-1}$)	Final biomass ($g\ L^{-1}$)	Total hydrogen (mL)
Batch process	1.00	0.60[a]	272
Variable volume fed-batch process	1.49	1.34	1529
Fixed volume fed-batch process	1.59	1.57	1560
Continuous process	1.50	1.50	1750

[a] Final biomass concentration in the batch process is measured at the 210th hour instead of the 750th hour.

Identifiability of the current system has not been considered in our work so far. In as much as it is desirable to know that the true values of parameters involved in a model can be known, constituting what model identifiability is, this aspect is rarely considered in biochemical reaction systems and more particularly it has not been considered in any of the numerous publications reviewed in producing the work presented here. While theoretically valuable, most work in the field of biochemical reaction systems adopts a practical approach where parameter values can be compared to published known values for individual kinetic mechanisms, estimated usually from different experimental setups and systems. From this point of view, the values we have estimated for kinetic parameters in this work is in relatively very good agreement with published values, as mentioned throughout the paper. Nonetheless future work needs to address this aspect rigorously as it plays an important role in obtaining reliable models for process systems.

Acknowledgements

The author D. Zhang gratefully acknowledges the support from his family, the author P. Dechatiwongse is supported by a scholarship from the Royal Thai Government, Thailand. Solar Hydrogen Project was funded by the UK Engineering and Physical Sciences Research Council (EPSRC), Project reference EP/F00270X/1. The author E.A. del Rio-Chanona funding by CONACyT Scholarship No. 522530 scholarship from the Secretariat of Public Education and the Mexican government. The authors wish to thank Mr. Fabio Fiorelli for his invaluable advice and support during the preparation of this work.

References

Alagesan, S., Gaudana, S., Krishnakumar, S., Wangikar, P., 2013. Model based optimization of high cell density cultivation of nitrogen-fixing cyanobacteria. Bioresour. Technol. 148, 228–233. ISSN 1873-2976. http://dx.doi.org/10.1016/j.biortech.2013.08.144 ⟨http://www.ncbi.nlm.nih.gov/pubmed/24047683⟩.

Antal, T.K., Krendeleva, T.E., Rubin, A.B., 2011. Acclimation of green algae to sulfur deficiency: underlying mechanisms and application for hydrogen production. Appl. Microbiol. Biotechnol. 89 (1), 3–15. ISSN 1432-0614. http://dx.doi.org/10.1007/s00253-010-2879-6 ⟨http://www.ncbi.nlm.nih.gov/pubmed/20878321⟩.

Bandyopadhyay, A., Stöckel, J., Min, H., Sherman, L.A., Pakrasi, H.B., 2010. High rates of photobiological H_2 production by a cyanobacterium under aerobic conditions. Nat. Commun. 1, 139. ISSN 2041-1723, http://dx.doi.org/10.1038/ncomms1139 ⟨http://www.ncbi.nlm.nih.gov/pubmed/21266989⟩.

Bezerra, M.A., Santelli, R.E., Oliveira, E.P., Villar, L.S., Escaleira, L.A., 2008. Response surface methodology (RSM) as a tool for optimization in analytical chemistry. Talanta 76 (5), 965–977. ISSN 1873-3573. http://dx.doi.org/10.1016/j.talanta.2008.05.019 ⟨http://www.ncbi.nlm.nih.gov/pubmed/18761143⟩.

Biegler, L.T., 2007. An overview of simultaneous strategies for dynamic optimization. Chem. Eng. Process.: Process Intensif. 46 (11) 1043–1053. ISSN 02552701. http://dx.doi.org/10.1016/j.cep.2006.06.021 ⟨http://linkinghub.elsevier.com/retrieve/pii/S0255270107001122⟩.

Biegler, L.T., 2010. Nonlinear Programming, Society for Industrial and Applied Mathematics. ISBN: 978-0-89871-702-0. http://dx.doi.org/10.1137/1.9780898719383 ⟨http://epubs.siam.org/doi/book/10.1137/1.9780898719383⟩.

Catalanotti, C., Yang, W., Posewitz, M., (May) 2013. Fermentation metabolism and its evolution in algae. Front. Plant Sci. 4, 150. ISSN 1664-462X. http://dx.doi.org/10.3389/fpls.2013.00150.

Cooke, P., Porter, J., Pinto, H., Cruz, A.R., Zhang, F., 2011. Notes from the Iberian Algae Belt. Eur. Plan. Stud. 19 (1), 159–173. http://dx.doi.org/10.1080/09654313.2011.525391, ISSN 0965-4313.

Dechatiwongse, P., Srisamai, S., Maitland, G., Hellgardt, K., 2014. Effects of light and temperature on the photoautotrophic growth and photoinhibition of nitrogen-fixing cyanobacterium Cyanothece sp. ATCC 51142. Algal Res. 5, 103–111. ISSN 22119264. http://dx.doi.org/10.1016/j.algal.2014.06.004 ⟨http://linkinghub.elsevier.com/retrieve/pii/S2211926414000563⟩.

Dechatiwongse, P., Maitland, G.C., Hellgardt, K., 2015. Enhancement in bio-hydrogen and biomass productivity of unicellular cyanobacterium Cyanothece using a two-stage chemostat photo-bioreactor system. Algal Res. (under review).

Fouchard, S., Pruvost, J., Degrenne, B., Titica, M., Legrand, J., 2009. Kinetic modeling of light limitation and sulfur deprivation effects in the induction of hydrogen production with Chlamydomonas reinhardtii: Part I. Model development and parameter identification. Biotechnol. Bioeng. 102 (1), 232–277. ISSN 1097-0290. http://dx.doi.org/10.1002/bit.22034 ⟨http://www.ncbi.nlm.nih.gov/pubmed/18688816⟩.

Hart, W.E., Laird, C., Waston, J.-P., Woodruff, D.L., 2012. Pyomo-Optimization Modeling in Python. Springer.

Klipp, E., Herwig, R., Kowald, A., Wierling, C., Lehrach, H., 2005. Systems Biology in Practice: Concepts, Implementation and Application. Wiley-VCH Verlag GmbH & Co. KGaA, Weinheim.

Kufryk, G., 2013. Advances in utilizing cyanobacteria for hydrogen production. Adv Microbiol 3 (6), 60–68.

Melis, A., Zhang, L., Forestier, M., 2000. Sustained photobiological hydrogen gas production upon reversible inactivation of oxygen evolution in the green alga *Chlamydomonas reinhardtii*. Plant Physiol. 122 (1), 127–136, ISSN 0032-0889.

Min, H., Sherman, L.A., 2010. Hydrogen production by the unicellular, diazotrophic cyanobacterium Cyanothece sp. strain ATCC 51142 under conditions of continuous light. Appl. Environ. Microbiol. 76 (13), 4293–4301. ISSN 1098-5336, http://dx.doi.org/10.1128/AEM.00146-10 ⟨http://www.pubmedcentral.nih.gov/articlerender.fcgi?artid=2897434&tool=pmcentrez&rendertype=abstract⟩.

Navarro, A., Vassiliadis, V., 2014. Computer algebra systems coming of age: dynamic simulation and optimization of DAE systems. Math. Comput. Chem. Eng. 62, 125–138. ISSN 00981354. http://dx.doi.org/10.1016/j.compchemeng.2013.11.004 ⟨http://linkinghub.elsevier.com/retrieve/pii/S0098135413003542⟩.

Obeid, J., Magnin, J., Flaus, J., Adrot, O., Willison, J., Zlatev, R., 2009. Modelling of hydrogen production in batch cultures of the photosynthetic bacterium

Rhodobacter capsulatus. Int. J. Hydrog. Energy 34 (1), 180–185. ISSN 03603199. http://dx.doi.org/10.1016/j.ijhydene.2008.09.081 ⟨http://linkinghub.elsevier.com/retrieve/pii/S0360319908011920⟩.

Provasoli, L., Mclaughlin, J.J., Droop, M.R., 1957. The development of artificial media for marine algae. Arch. Mikrobiol. 25 (4), 392–428. ISSN 0003-9276. ⟨http://www.ncbi.nlm.nih.gov/pubmed/13403656⟩.

Tamburic, B., Zemichael, F.W., Maitland, G.C., Hellgardt, K., 2012. A novel nutrient control method to deprive green algae of sulphur and initiate spontaneous hydrogen production. Int. J. Hydrog. Energy 37 (11), 8988–9001. ISSN 03603199. http://dx.doi.org/10.1016/j.ijhydene.2012.02.043⟨http://linkinghub.elsevier.com/retrieve/pii/S0360319912003655⟩.

Tamburic, B., Dechatiwongse, P., Zemichael, F.W., Maitland, G.C., Hellgardt, K., 2013. Process and reactor design for biophotolytic hydrogen production. Phys. Chem. Chem. Phys.: PCCP 15 (26), 10783–10794. ISSN 1463-9084. http://dx.doi.org/10.1039/c3cp51866c ⟨http://www.ncbi.nlm.nih.gov/pubmed/23689756⟩.

Tripp, H.J., Bench, S.R., Turk, K.A., Foster, R.A., Desany, B.A., Niazi, F., Affourtit, J.P., Zehr, J.P., 2010. Metabolic streamlining in an open-ocean nitrogen-fixing cyanobacterium. Nature 464 (7285), 90–4. ISSN 1476-4687, http://dx.doi.org/10.1038/nature08786 ⟨http://www.ncbi.nlm.nih.gov/pubmed/20173737⟩.

Vatcheva, I., de Jong, H., Bernard, O., Mars, N.J.I., 2006. Experiment selection for the discrimination of semi-quantitative models of dynamical systems. Artif. Intell. 170 (4–5), 472–506. ISSN 00043702. http://dx.doi.org/10.1016/j.artint.2005.11.001 ⟨http://linkinghub.elsevier.com/retrieve/pii/S0004370205002092⟩.

Wächter, A., Biegler, L.T., 2005. On the implementation of an interior-point filter line-search algorithm for large-scale nonlinear programming, vol. 106. ISBN 1010700405. http://dx.doi.org/10.1007/s10107-004-0559-y ⟨http://link.springer.com/10.1007/s10107-004-0559-y⟩.

Xie, G., Liu, B., Xing, D., Ding, J., Nan, J., Ren, H., Guo, W., Ren, N., 2012. The kinetic characterization of photofermentative bacterium Rhodopseudomonas faecalis RLD-53 and its application for enhancing continuous hydrogen production. Int. J. Hydrog. Energy 37 (18), 13718–13724. http://dx.doi.org/10.1016/j.ijhydene.2012.02.168, ISSN 03603199.

Zhang, D., Xiao, N., Mahbubani, K.T., del Rio-Chanona, E.A., Slater, N.K.H., Vassiliadis, V.S., Kinetic modelling of biohydrogen production by Rhodopseudomonas palustris: model development and effects of glutamate and operating conditions on hydrogen production and glycerol conversion efficiency. Chem. Eng. Sci. (under review).

Zhang, D., Dechatiwongse, P., Hellgardt, K., 2015. Modelling light transmission, cyanobacterial growth kinetics and fluid dynamics in a laboratory scale multi-phase photo-bioreactor for biological hydrogen production. Algal Res. 8, 99–107.